



Qualification of innovative floating substructures for 10MW wind turbines and water depths greater than 50m

Project acronym LIFES50+
Grant agreement 640741
Collaborative project
Start date 2015-06-01
Duration 40 months

Deliverable D4.5 State-of-the-art models for the two LIFES50+ 10MW floater concepts

Lead Beneficiary DTU
Due date 2017-08-31
Delivery date 2018-04-19
Dissemination level Public
Status Final
Classification Unrestricted

Keywords Numerical models, state-of-the-art, floating wind turbines
Company document number Click here to enter text.



The research leading to these results has received funding from the European Union Horizon2020 programme under the agreement H2020-LCE-2014-1-640741.

Disclaimer

The content of the publication herein is the sole responsibility of the publishers and it does not necessarily represent the views expressed by the European Commission or its services.

While the information contained in the documents is believed to be accurate, the authors(s) or any other participant in the LIFES50+ consortium make no warranty of any kind with regard to this material including, but not limited to the implied warranties of merchantability and fitness for a particular purpose.

Neither the LIFES50+ Consortium nor any of its members, their officers, employees or agents shall be responsible or liable in negligence or otherwise howsoever in respect of any inaccuracy or omission herein.

Without derogating from the generality of the foregoing neither the LIFES50+ Consortium nor any of its members, their officers, employees or agents shall be liable for any direct or indirect or consequential loss or damage caused by or arising from any information advice or inaccuracy or omission herein.

Document information

Version	Date	Description
1	2018-01-31	<p>Draft</p> <p>Prepared by Pegalajar-Jurado, A.; Madsen, F.J.; Borg, M.; Bredmose, H.;</p> <p>Reviewed by Enter names</p> <p>Approved by Enter names</p>
2	2018-02-28	<p>Draft for review</p> <p>Prepared by Pegalajar-Jurado, A.; Madsen, F.J.; Borg, M.; Bredmose, H.;</p> <p>Reviewed by Matha D., Straume J.G., Galvan-Fernandez J.</p> <p>Approved by Enter names</p>
3	2018-03-24	<p>Draft for review</p> <p>Prepared by Pegalajar-Jurado, A.; Madsen, F.J.; Borg, M.; Bredmose, H.;</p> <p>Reviewed by Galvan-Fernandez J.</p> <p>Approved by Bredmose, H.</p>
4	2018-04-13	<p>Final version</p> <p>Prepared by Pegalajar-Jurado, A.; Madsen, F.J.; Borg, M.; Bredmose, H.;</p> <p>Reviewed by Bredmose, H.</p> <p>Approved by Bredmose, H.</p>
Final	2018-04-16	<p>Final version for QA before submission</p> <p>Prepared by Pegalajar-Jurado, A.; Madsen, F.J.; Borg, M.; Bredmose, H.;</p> <p>Reviewed by Jan Norbeck.</p> <p>Approved by Petter Andreas Berthelsen</p>



Authors	Organization
Pegalajar-Jurado, A.	DTU
Madsen, F.J.	DTU
Borg, M.	DTU
Bredmose, H.	DTU

Contributors	Organization
Mirzaei, M.	DTU
Yu, W.	University of Stuttgart
Müller, K.	University of Stuttgart
Lemmer, F.	University of Stuttgart
Straume, J.G.	Olav Olsen
Landbø, T.	Olav Olsen
Andersen, H.S.	Olav Olsen
Galvan-Fernandez, J.	Tecnalia
Perez-Moran, G.	Tecnalia
Sanchez-Lara, M.J.	Tecnalia

Definitions & Abbreviations

PI	Proportional-Integral
NREL	National Renewable Energy Laboratory
WP	Work Package
RWT	Reference Wind Turbine
FAST	Fatigue, Aerodynamics, Structures and Turbulence
SWL	Still water level
CM	Centre of mass
AP	Anchor point
FLP	Fairlead point
CP	Connection point
DoF	Degree of freedom
DLC	Design Load Case
PSD	Power spectral density



Executive Summary

This report describes the implementation in FAST of the DTU 10MW Reference Wind Turbine mounted on two floating substructures, namely the LIFES50+ OO-Star Wind Floater Semi 10MW and the NAUTILUS-10 floating substructure. The two floating substructures and turbine configurations are defined in [1] and the present numerical implementations are consistent with those definitions. FAST v8.16 is selected as the version for implementation of the state-of-the-art models. The purpose of this implementation is to serve as a reference for different activities carried out by partners within the project consortium, and also to provide realistic reference models for public use outside of LIFES50+. The land-based wind turbine structural and aerodynamic models were already implemented in FAST within the LIFES50+ project [2]. In this report, attention is given to the changes necessary to adapt the FAST model to the two floating substructures. These changes entail controller, tower structural properties, floating substructure hydrodynamics and mooring system. The basic DTU Wind Energy controller was tuned by the developers of each floating concept, in order to avoid the “negative damping” problem. The tower in one of the models is defined down to the still water level to capture some of the floating substructure flexibility. The mooring lines are implemented in the FAST module MoorDyn, which is a dynamic lumped-mass mooring line model that allows the user to define multi-segmented mooring lines. Hydrodynamics properties (hydrostatic stiffness matrix, frequency-dependent added mass and radiation damping matrices, and frequency-dependent vector of wave excitation forces) are precomputed in the radiation-diffraction solver WAMIT for both floating substructures, and transformed to time domain by convolution. Viscous effects, not captured by radiation-diffraction theory, are captured internally in Hydro-Dyn by inclusion of the Morison drag term for the OO-Star Semi floating substructure, while they are modelled through linear and quadratic global damping matrices for the NAUTILUS-10 floating substructure. A first set of simulations for system identification purposes is carried out to assess system properties such as static offset, natural frequencies and response to regular waves. The controller is tested in a simulation with uniform wind ranging from cut-in to cut-out wind speed. A set of simulations in stochastic wind and waves is carried out to characterize the global response of both floating substructures, showing that the models behave as expected. The results are presented and the main physical phenomena are discussed. Finally, accessibility and referencing information for the two public models is given.



Contents

1	Introduction	6
2	Reference wind turbine and controller	7
2.1	Wind turbine.....	7
2.2	Controller.....	7
3	Modelling approach.....	8
3.1	Approach for hydrodynamic modelling	8
3.2	Approach for modelling of the mooring system.....	9
4	Selection of load cases	10
5	Numerical model of the OO-Star Wind Floater Semi 10MW	11
5.1	Modelling of the tower	11
5.2	Modelling of the mooring system.....	14
5.3	Modelling of the hydrodynamics.....	14
5.4	System identification.....	20
5.5	Response to wind and waves	23
6	Numerical model of the NAUTILUS-DTU10 floating wind turbine.....	26
6.1	Modelling of the tower	26
6.2	Modelling of the mooring system.....	27
6.3	Modelling of the hydrodynamics.....	27
6.4	System identification.....	31
6.5	Response to wind and waves	34
7	Model accessibility and referencing	37
8	Conclusions	37
9	References	38
10	Appendix	40
10.1	Inclusion of Morison drag in the LIFES50+ NAUTILUS-10 floating substructure	40



1 Introduction

This report describes the implementation in FAST of the DTU 10MW Reference Wind Turbine mounted on the two floating substructures described in LIFES50+ D4.2 [1], namely the LIFES50+ OO-Star Wind Floater Semi 10MW and the NAUTILUS-10 floating substructure. FAST v8.16, an aero-hydro-servo-elastic numerical tool developed by the National Renewable Energy Laboratory (NREL), was selected for the implementation of the state-of-the-art numerical models. The purpose of this implementation is to serve as a reference for the different activities carried out by partners within the project consortium and their respective Work Packages (WP), in particular:

- Hybrid physical model testing in WP3, where a hardware-in-the-loop approach is used to exert rotor loads on a physical model of the floating substructure and turbine tower with a top mass, tested physically in the ocean basin at SINTEF Ocean; and where a hardware-in-the-loop controlled hexafloat is used to drive real-time simulated motion of the tower bottom for a physical model of the tower and rotor in the wind tunnel at Politecnico di Milano.
- Model validation in WP4, where the accuracy of the present state-of-the-art numerical models is screened against experimental results and compared to the performance of simpler models.
- Work in WP7 on the model accuracy and its design implications.

The wind turbine structural and aerodynamic models for an onshore configuration have already been implemented in FAST, as described in LIFES50+ D1.2 [2]. In the present report, attention is given to the changes necessary to adapt the FAST model of the onshore DTU 10MW Reference Wind Turbine to each of the two floating foundations. These changes entail controller, tower structural properties, floating substructure hydrodynamics and mooring system.

First, the wind turbine and controller are briefly described in Section 2. General considerations on the modelling approach are detailed in Section 3, while a selection of load cases is presented in Section 4. Sections 5 and 6 present the specific modelling considerations and discussion of key results for the two floating substructures. Finally, information about accessibility and referencing to the models is given in Section 7, and some general conclusions are stated in Section 8.



2 Reference wind turbine and controller

2.1 Wind turbine

The DTU 10MW Reference Wind Turbine (RWT) is described in [3] (see Figure 1). For the present numerical models, the turbine is installed on each of the two-selected public floating substructure concepts. To account for the freeboard of the floating substructure and to maintain the hub height at 119 m, the turbine tower was shortened for both floating substructures, as detailed in [1]. Further, the FAST implementation of the land-based configuration of the DTU 10MW RWT is described in [2].



Figure 1: DTU 10MW RWT

2.2 Controller

The DTU 10MW RWT is here installed on a floating substructure. Therefore, the baseline onshore controller cannot be used here due to the “negative damping” problem (see, for example, [4]). In LIFES50+ the basic DTU Wind Energy controller is employed [5]. The DTU controller consists of two different controllers for the partial load region (i.e. operation below rated wind speed) and the full load region (i.e. operation above rated wind speed), and a mechanism that smoothly switches between these two controllers around rated wind speed. Details of the controller can be found in [5]. The pole-placement method [6] was used to tune the proportional-integral (PI) controllers where needed. The OO-Star Semi controller was tuned by Dr. techn. Olav Olsen AS. The NAUTILUS-DTU10 controller was initially tuned at DTU and further tuned by Tecnalia Research & Innovation later [7]. The controller performance will be shown and discussed later in this report, although details on the controller tuning approach are not included in this document.



3 Modelling approach

The numerical models are implemented in the aero-hydro-servo-elastic tool FAST v8.16.00a-bjj [8]. FAST (Fatigue, Aerodynamics, Structures and Turbulence), developed at NREL through U.S. Department of Energy support, is an open-source multi-physics tool practical to the engineering design of wind turbines, including both bottom-fixed and floating offshore wind turbines [9]. For the present work, the FAST model of the onshore DTU 10MW RWT [2] has been adapted to the two floating substructures. To avoid redundancy, only the changes made to the FAST model of the onshore wind turbine will be described here. These changes entail modelling of the tower, hydrodynamics and mooring system, as well as tuning of the controller. All the information necessary to establish the FAST models was provided by Dr. techn. Olav Olsen AS and Nautilus Floating Solutions SL (through Tecnalia Research & Innovation [7]), respectively. A close dialogue between LIFES50+ WP4 and the two concept developers has been maintained throughout the process of defining the two FAST models presented here.

3.1 Approach for hydrodynamic modelling

3.1.1 First-order radiation-diffraction hydrodynamics

When modelling a floating wind turbine in FAST, it is common practice to first compute the hydrodynamic properties of the floating substructure in a radiation-diffraction, frequency-domain, potential-flow solver such as WAMIT [10], and to couple these frequency-domain results to the time-domain model through the Cummins equation [11]. These hydrodynamic properties are the hydrostatic restoring matrix \mathbf{C}_{hst} , the hydrodynamic added mass matrix $\mathbf{A}(\omega)$ and radiation damping matrix $\mathbf{B}(\omega)$, and the vector of wave diffraction forces $\mathbf{X}(\omega)$. The reader should note that added mass, radiation damping and wave diffraction forces depend on the angular frequency, ω , and that all properties are computed with respect to the point of flotation. These properties, together with the floating substructure inertia matrix \mathbf{M} , the Fourier coefficients for the floating substructure motion in 6 degrees of freedom (DoF) $\hat{\xi}(\omega)$ and the Fourier coefficients of the incident wave surface elevation $\hat{\eta}(\omega)$, define the equation of motion for an unrestrained, floating body in the frequency domain:

$$[-\omega^2(\mathbf{M} + \mathbf{A}(\omega)) + i\omega\mathbf{B}(\omega) + \mathbf{C}_{hst}]\hat{\xi}(\omega) = \mathbf{X}(\omega)\hat{\eta}(\omega) \quad (1)$$

Further details on the radiation-diffraction theory and its coupling to FAST can be found in [12] and [9], respectively.

3.1.2 Viscous effects

Viscous drag is not captured by potential-flow solvers. Therefore, it needs to be modelled separately within the FAST model. This is usually done by inclusion of the drag term in the Morison equation, which provides the transversal drag force df_{drag} on a cylindrical member section of length dz :

$$df = \frac{1}{2}\rho C_D D v_{rel} |v_{rel}| dz \quad (2)$$

Here ρ is the fluid density, C_D is an appropriate drag coefficient, D is the cylinder diameter, and v_{rel} is the relative velocity between the body and the fluid, projected to the normal of the cylinder axis. Analogously, the axial drag on a circular heave plate is computed as:

$$F = \frac{1}{2}\rho C_{DHP} A_{HP} v_{rel} |v_{rel}| \quad (3)$$



where C_{DHP} is a drag coefficient and A_{HP} is the heave plate area projected on the plane normal to the motion.

When modelling viscous drag in FAST, it is important to consider that HydroDyn only allows the user to define cylindrical members, and that the axial loads applied at the member ends are referred to the member cross-section properties at that particular end. In addition, HydroDyn assumes that the axial drag on a heave plate is modelled with two joints (one at each side of the heave plate), and half of the force given by Eq. (3) is applied at each side. If only one joint is employed, the axial drags coefficients have to be doubled accordingly.

Alternatively, viscous effects can be modelled through linear and quadratic damping matrices lumped at the center of flotation, which need to be obtained from experiments or higher-fidelity models. This approach only considers the floating substructure global velocity instead of the relative velocity between the structure and the fluid, therefore the viscous forcing part of the Morison equation is not modelled (see Eq. (2)).

3.1.3 Approach to varying equilibrium position over load cases

Generally, a floating wind turbine will oscillate around different equilibrium positions for different environmental conditions. Ideally, one would compute radiation-diffraction properties for each equilibrium position and use the corresponding WAMIT data for each environmental condition. Here, however, we followed a simpler approach where hydrostatic and hydrodynamic properties for each floating substructure were computed for a single reference position, which corresponds to the floating structure in calm water and with no wind. These WAMIT files were used for all the simulations presented in this document.

3.2 Approach for modelling of the mooring system

The standard version of FAST includes several options for the modelling of mooring lines [13]. Quasi-static mooring loads can be included with the mooring module MAP++. FEAMooring is able to model dynamic effects such as line mass inertia, buoyancy, and hydrodynamic forces from the Morison equation (assuming still water, but considering the kinematics of the mooring line at each time step). However, FEAMooring does not allow multi-segmented mooring lines or clump weights. The mooring module MoorDyn [14] provides the option of multi-segmented lines and clump weights, necessary for the correct modelling of the OO-Star Semi mooring lines. MoorDyn also captures dynamic effects, but the hydrodynamic loads are also applied to a mooring line moving in still water. Finally, the hydrodynamic loads from incident waves can be modelled by using FAST together with the commercial tool OrcaFlex. For the present work, to be able to correctly model the OO-Star Semi's multi-segment mooring lines, while still keeping the models open-source, the MoorDyn module was chosen.



4 Selection of load cases

A set of representative load cases was selected with the purpose of testing and demonstrating the two models. In Table 1, load cases 1-8 (system identification) are of diagnostic nature, while 9-15, 16-17 and 18 (response to wind and waves) are representative of Design Load Case (DLC) 1.2, 1.6 and 6.1, respectively. As specified in [15] for the Gulf of Maine, the wind turbulence has been set to Class C for load cases 9-18, and a Pierson-Moskowitz spectrum was used for the irregular sea states. These load cases were run for 5400 s to be able to remove 1800 s of transient (given the long surge natural period for both floating substructures), and the same turbulence boxes with a duration of 5400 s are used for both models. The wave conditions for load cases 16-18 correspond to the 50-year significant wave height and the upper limit of the 50-year peak period range [15]. The wind speed values refer to the mean speed at hub height. The wind turbine was parked (i.e. fixed rotor) for the cases with no wind and operating with active control otherwise (except for case #18, where it is parked and the blades are feathered).

Table 1: Summary of simulations carried out with the two FAST models

#	Name	Duration [s]	Waves	Wind	Wind turbine
1	Static equilibrium	1000	-	-	Parked
2	Surge decay	1000	-	-	Parked
3	Heave decay	1000	-	-	Parked
4	Pitch decay	1000	-	-	Parked
5	Yaw decay	1000	-	-	Parked
6	Tower decay	1000	-	-	Parked
7	Regular wave	1800	Regular $H=6\text{ m}$, $T=10\text{ s}$	-	Parked
8	Step wind	15000	-	Uniform, steady 4-25 m/s	Operating Active control
9	Operational 1	5400	Irregular $H_s=1.38\text{ m}$, $T_p=7.0\text{ s}$	Turbulent 5.0 m/s	Operating Active control
10	Operational 2	5400	Irregular $H_s=1.67\text{ m}$, $T_p=8.0\text{ s}$	Turbulent 7.1 m/s	Operating Active control
11	Operational 3	5400	Irregular $H_s=2.20\text{ m}$, $T_p=8.0\text{ s}$	Turbulent 10.3 m/s	Operating Active control
12	Operational 4	5400	Irregular $H_s=3.04\text{ m}$, $T_p=9.5\text{ s}$	Turbulent 13.9 m/s	Operating Active control
13	Operational 5	5400	Irregular $H_s=4.29\text{ m}$, $T_p=10.0\text{ s}$	Turbulent 17.9 m/s	Operating Active control
14	Operational 6	5400	Irregular $H_s=6.20\text{ m}$, $T_p=12.5\text{ s}$	Turbulent 22.1 m/s	Operating Active control
15	Operational 7	5400	Irregular $H_s=8.31\text{ m}$, $T_p=12.0\text{ s}$	Turbulent 25.0 m/s	Operating Active control
16	Ultimate 1	5400	Irregular $H_s=10.90\text{ m}$, $T_p=16.0\text{ s}$	Turbulent 7.1 m/s	Operating Active control
17	Ultimate 2	5400	Irregular $H_s=10.90\text{ m}$, $T_p=16.0\text{ s}$	Turbulent 22.1 m/s	Operating Active control
18	Extreme	5400	Irregular $H_s=10.90\text{ m}$, $T_p=16.0\text{ s}$	Turbulent 44.0 m/s	Parked Blades feathered



5 Numerical model of the OO-Star Wind Floater Semi 10MW

The LIFES50+ OO-Star Wind Floater Semi 10MW (see Figure 2), is extensively described in [1]. Some of the main properties are collected in Table 2 below. For brevity, through this report sometimes the LIFES50+ OO-Star Wind Floater Semi 10MW will be referred to as “OO-Star Semi”.

Table 2: Main properties of the OO-Star Semi floating substructure

Type	Material	Draft	Freeboard	Displaced volume	Floating substructure mass
		[m]	[m]	[m ³]	[kg]
Semisubmersible	Post-tensioned concrete	22.00	11.00	2.3509E+04	2.1709E+07



Figure 2: The OO-Star Semi floating substructure. Figure provided by Dr. techn. Olav Olsen AS

5.1 Modelling of the tower

FAST allows the user to model flexible tower, blades and mooring lines, whereas the floating substructure is modelled as a rigid body (*rigid* approach). Hence, when modelling a floating wind turbine in FAST, it is common practice to model the tower as a flexible beam extending from the nacelle to the interface between the tower and the floating substructure. However, the substructure flexibility is known to have an impact on the system natural frequencies and response (see, for example, [1] and [16]). Other aero-hydro-elastic tools include a full structural model of the turbine and floating substructure (*flexible* approach). To capture some of the floating substructure flexibility, for the FAST model of the OO-Star Semi floating substructure presented here the portion of substructure between still water level (SWL) and tower interface has been modelled as part of the tower (*semi-flexible* approach). The *semi-flexible* approach entails extending the definition of the tower to SWL, and adding one more tower section (tower



section 0) to the tables of tower properties given in [1]. Table 3 below shows the properties of the added section, which has constant diameter for simplicity. Even though the OO-Star Semi floating substructure has a central column that is tapered from SWL to a height of 2.775 m, structural details of the internal design (e.g. wall thickness) are not available and a straight cylinder has been used instead, with the specified values of mass and stiffness properties. This simplification only affects the modelling of the tower, as the tapering of the columns is included in the hydrodynamic model.

Table 3: Properties of tower section 0, added to the tower definition in the FAST model of the OO-Star Semi

Section height	Outer diameter	Mass density	EA	EI	GJ
[m]	[m]	[kg/m]	[N]	[N m ²]	[N m ²]
11.00	12.050	5.7600E+04	5.9600E+11	9.8800E+12	8.2300E+12

Since a part of the floating substructure has been modelled as part of the tower, the original inertia properties of the floating substructure need to be modified accordingly (see Figure 3). The original floating substructure is defined by a mass m_p , a vertical centre of mass CM_p located at a height z_p , a pitch/roll mass moment of inertia I_{yp} and a yaw mass moment of inertia I_{zp} . The portion of floating substructure modelled as tower (tower section 0) corresponds to m_0 , CM_0 , z_0 , I_{y0} and I_{z0} . Hence, the new inertia properties for the floating substructure (denoted here with p') can be obtained by solving the equations below, which assure conservation of total mass, CM and mass moment of inertia.

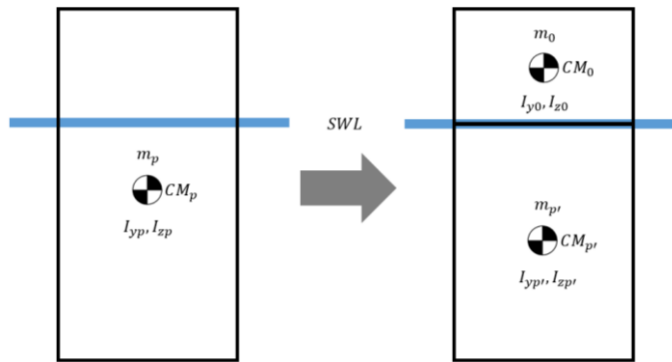


Figure 3: Sketch of original and modified floating substructure inertia properties

$$m_p = m_{p'} + m_0 \quad (4)$$

$$m_p z_p = m_{p'} z_{p'} + m_0 z_0 \quad (5)$$

$$I_{yp}^{CMp'} = I_{yp'}^{CMp'} + I_{y0}^{CMp'} \quad (6)$$

$$I_{zp} = I_{zp'} + I_{z0} \quad (7)$$

The superscript CM_p , in Eq. (6) indicates that all pitch/roll mass moments of inertia in the equation need to be referred to the new floating substructure centre of mass $CM_{p'}$, because the floating substructure mass moment of inertia in FAST is given with respect to the floating substructure CM, which has



changed from CM_p to $CM_{p'}$. This can be done by using the parallel axis theorem. For instance, the original floating substructure pitch/roll inertia about the original CM_p can be referred to the new $CM_{p'}$ by virtue of:

$$I_{yp}^{CMp'} = I_{yp}^{CMp} + m_p(z_p - z_{p'})^2 \quad (8)$$

Table 4 below shows the original and the modified floating substructure inertia properties, as well as the original and modified tower length.

Table 4: Original and modified properties for the FAST model of the OO-Star Semi

	Tower length	Floating sub-structure mass	Floating sub-structure CM below MSL	Floating sub-structure pitch/roll inertia about CM	Floating sub-structure yaw inertia about CM
	[m]	[kg]	[m]	[kg m ²]	[kg m ²]
Original	104.63	2.1709E+07	15.225	9.4300E+09	1.6300E+10
Modified	115.63	2.1075E+07	15.848	9.1328E+09	1.6279E+10

For the FAST model presented here (*semi-flexible* approach), the mode shapes of the blades were computed in BModes using a cantilever boundary condition [2]. The mode shapes of the tower (including tower section 0) were computed in BModes with a cantilever boundary condition as well, and with the rotor-nacelle assembly represented by a point mass and inertia. With this approach, the coupled tower natural frequency obtained in FAST was 0.746 Hz. According to [1], the tower natural frequency in FAST is 0.786 Hz considering a completely rigid floating substructure (*rigid* approach). The difference in tower frequency observed between these two FAST models (0.746 Hz vs. 0.786 Hz) is due to the flexibility of the portion of the floating substructure above SWL (tower section 0). If a fully flexible structural model of the whole floating wind turbine is considered (*flexible* approach), the tower natural frequency is reported as 0.56 Hz in [1], obtained with a 3DFloat model.

A closer analysis of the natural frequencies was carried out. Two dominant fore-aft modes were found by eigenvalue analysis in the *flexible* 3DFloat model. These modes are compared in Table 5 to the frequencies seen in a spectral analysis of the tower response for a tower decay test in the *semi-flexible* FAST model.

Table 5: Mode types and natural frequencies with 3DFloat and FAST models

Mode	Frequencies seen in eigenmode analysis with <i>flexible</i> model [Hz]	Mode type in <i>flexible</i> model	Frequencies seen in decay test with <i>semi-flexible</i> model [Hz]
A	0.56	The top blade moves in phase with the tower, and the two lower blades move in anti-phase with the tower	0.579
B	0.70	The three blades move collectively, in anti-phase with the tower	0.746



From the results, there is thus overall agreement between the natural frequencies observed in the two models. The deviations are likely due to i) floater flexibility; ii) the detection method of natural frequency (eigenanalysis method / decay test method); and iii) the approach to structural modelling in the two solvers.

Further, and perhaps linked to these effects, it was found that the two models are dominated by different modes in time-domain simulations. Mode “A” was found to dominate in the 3DFloat *flexible* model, while mode “B” was found to dominate in the *semi-flexible* FAST model. For the FAST model, it was further confirmed that the dominant mode type (the three blades move collectively, in anti-phase with the tower) was consistent with the mode “B” of the 3DFloat model. While the two models were thus found to have quite close natural frequencies, the apparent difference in the dominantly excited mode in time-domain simulations is left for future investigation.

In conclusion, caution is necessary in the modelling of the tower-floating substructure coupled frequencies and awareness of the discrepancy between the excited tower modes predicted by the two models is necessary. A difference in tower frequency is important since the natural frequency is a design- and cost driver for the tower design. A wrong determination can thus lead to errors in the fatigue prediction and affect the structural lifetime.

5.2 Modelling of the mooring system

The mooring line properties for the OO-Star Semi floating substructure are defined in [1]. In the FAST model, six lines are defined; one line between each anchor point (AP) and connection point (CP), and one more between each CP and fairlead point (FLP), as summarized in Table 6 below. A clump mass of 50000 kg (effective mass in water) is included at each CP.

Table 6: Mooring lines for the OO-Star Semi floating substructure

Line #	Anchor coordinates			Connection coordinates			Fairlead coordinates		
	X	Y	Z	X	Y	Z	X	Y	Z
	[m]	[m]	[m]	[m]	[m]	[m]	[m]	[m]	[m]
1	-691	0	-130	-117.9	0	-81.1	-	-	-
2	345.5	598.42	-130	58.95	102.10	-81.1	-	-	-
3	345.5	-598.42	-130	58.95	-102.10	-81.1	-	-	-
4	-	-	-	-117.9	0	-81.1	-44	0	9.5
5	-	-	-	58.95	102.10	-81.1	22	38.11	9.5
6	-	-	-	58.95	-102.10	-81.1	22	-38.11	9.5

The number of segments was set to 80 for the lower part (lines 1, 2 and 3 between AP and CP, 585 m long) and to 20 for the upper part (lines 4, 5 and 6 between CP and FLP, 118 m long). The line internal damping ratio was set to 1, as recommended in the MoorDyn User’s Guide [14].

5.3 Modelling of the hydrodynamics

5.3.1 First-order radiation-diffraction hydrodynamics

The hydrostatic restoring matrix, referred to the centre of flotation and assuming centred CM of the rotor-nacelle assembly, is presented in Table 7. The hydrostatic matrix shown here was computed in



WAMIT and only includes the effects of water plane area and buoyancy, since the mass contributions are internally computed by FAST.

Table 7: Hydrostatic restoring matrix for the OO-Star Semi floating substructure

	1 (Surge)	2 (Sway)	3 (Heave)	4 (Roll)	5 (Pitch)	6 (Yaw)
1 (Surge)	0	0	0	0	0	0
2 (Sway)	0	0	0	0	0	0
3 (Heave)	0	0	5.3524E+06	0	2.1871E+05	0
4 (Roll)	0	0	0	-4.2089E+08	0	-1.6993E+04
5 (Pitch)	0	0	2.1871E+05	0	-4.1280E+08	0
6 (Yaw)	0	0	0	0	0	0

The added mass, radiation damping and wave diffraction forces (for zero degrees wave heading) for the OO-Star Semi floating substructure computed using WAMIT are shown in Figure 4, Figure 5 and Figure 6 respectively.

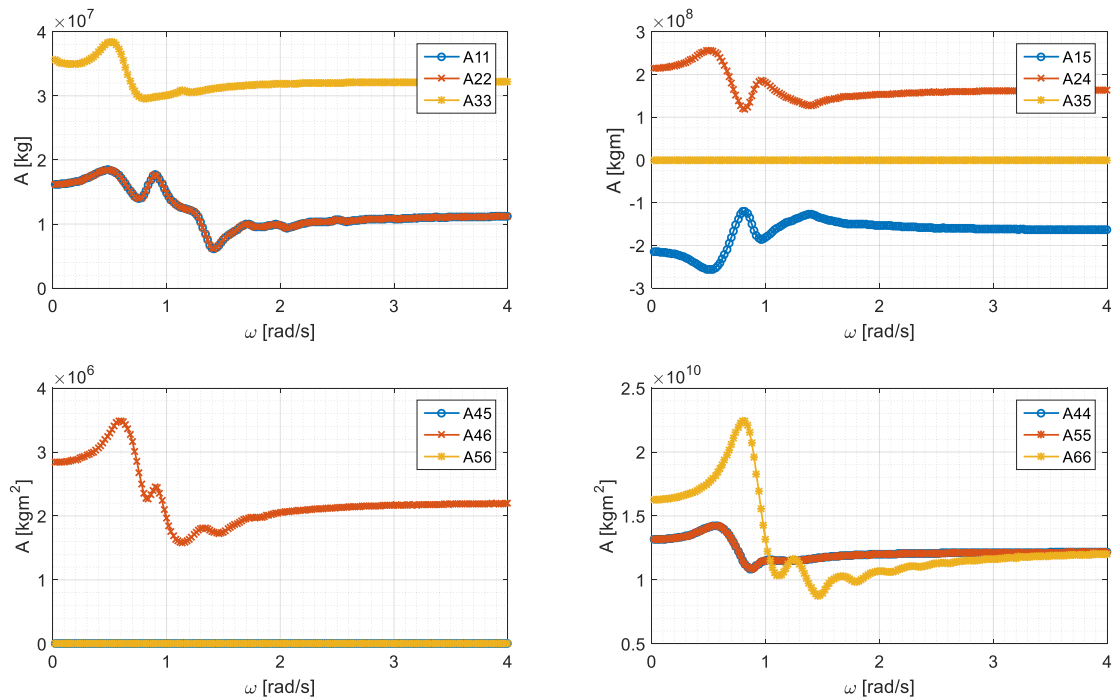


Figure 4: Added mass for the OO-Star Semi floating substructure



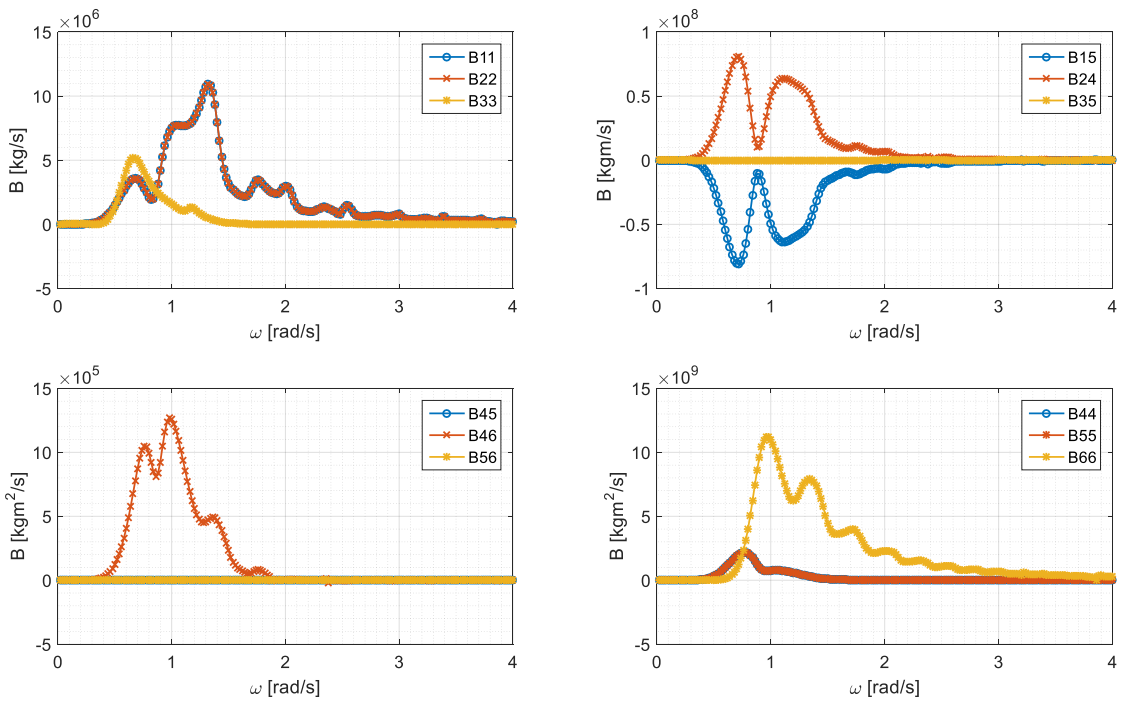


Figure 5: Radiation damping for the OO-Star Semi floating substructure

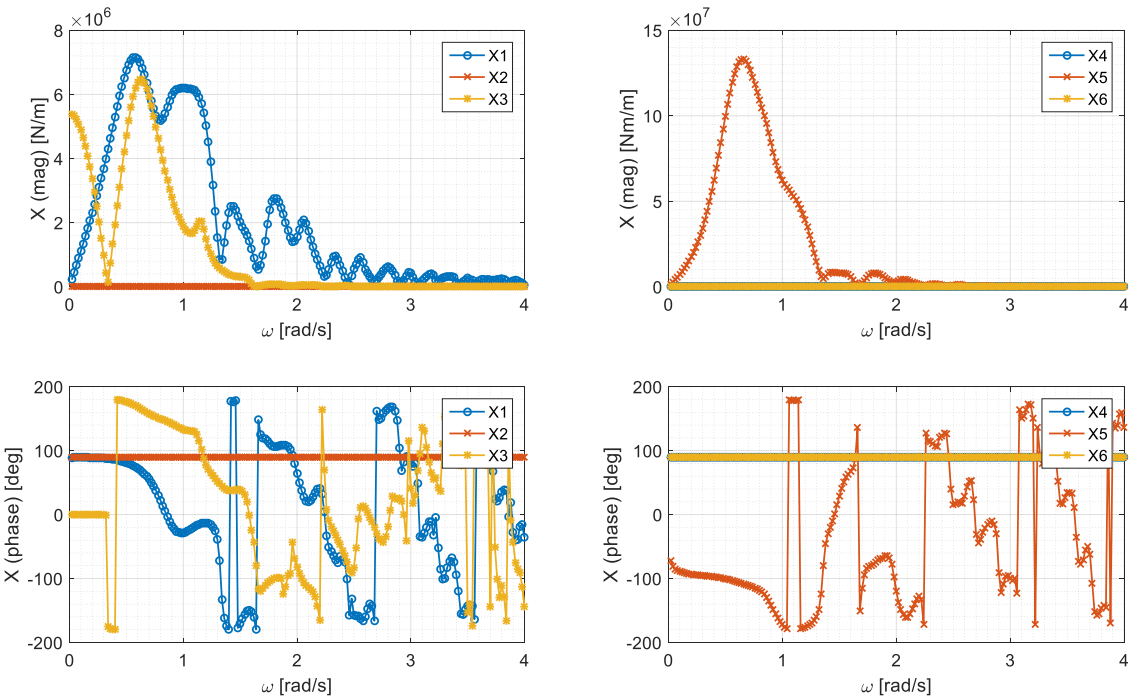


Figure 6: Wave diffraction forces for the OO-Star Semi floating substructure, magnitude (top) and phase (bottom)



5.3.2 Viscous effects

Viscous effects on the OO-Star Semi floating substructure are modelled through the Morison equation. Therefore, 14 members are defined as follows (see Figure 7). The floating substructure was considered brand new, therefore no marine growth effects were included, although for the design process they must be taken into account.

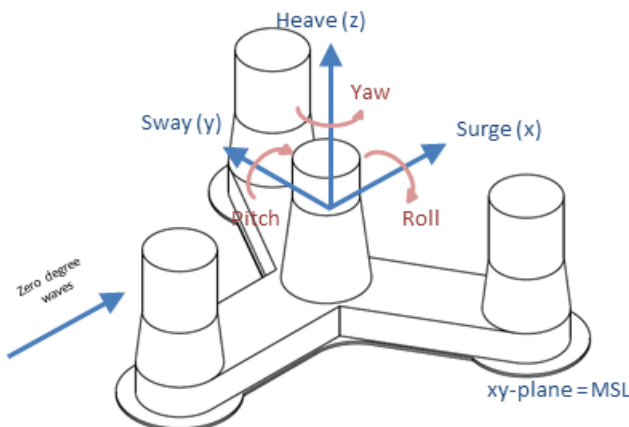


Figure 7: Geometry of the OO-Star Semi floating substructure [1]

Central vertical column

- One member corresponds to the upper section of the central column, with a transversal drag coefficient C_D of 0.729 [1] together with the physical column diameter D of 12.05 m.
- One member models the tapered bottom section of the central column, with a variable transversal drag coefficient C_D between 0.729 and 0.704 [1] and a variable diameter D between 12.05 and 16.2 m. This member extends down to the top of the star-shaped pontoon.

Outer vertical columns

- Three members correspond to the upper sections of the three outer columns, with a transversal drag coefficient C_D of 0.720 [1] and the physical column diameter D of 13.4 m.
- Three members represent the tapered bottom sections of the three outer columns, with a variable transversal drag coefficient C_D between 0.720 and 0.706 [1] together with a variable diameter D between 13.4 and 15.8 m. These members extend down to the top of the star-shaped pontoon.
- Three members represent the circular ends of the pontoon legs, with a transversal drag coefficient C_D of 0.706 [1] together with a diameter D of 15.8 m. These members extend from the bottom of the outer tapered columns to the heave plates.

The last three members, which represent the legs of the star-shaped pontoon, are defined to approximate the main drag loads on the real structure, but taking into account that HydroDyn only allows the definition of cylindrical members. A sketch of the physical and the model representation of the pontoon and slab is presented in Figure 8. The properties of the cylindrical members and heave plates that represent the star-shaped pontoon and slab in the FAST model are described below and summarized in Table 8.



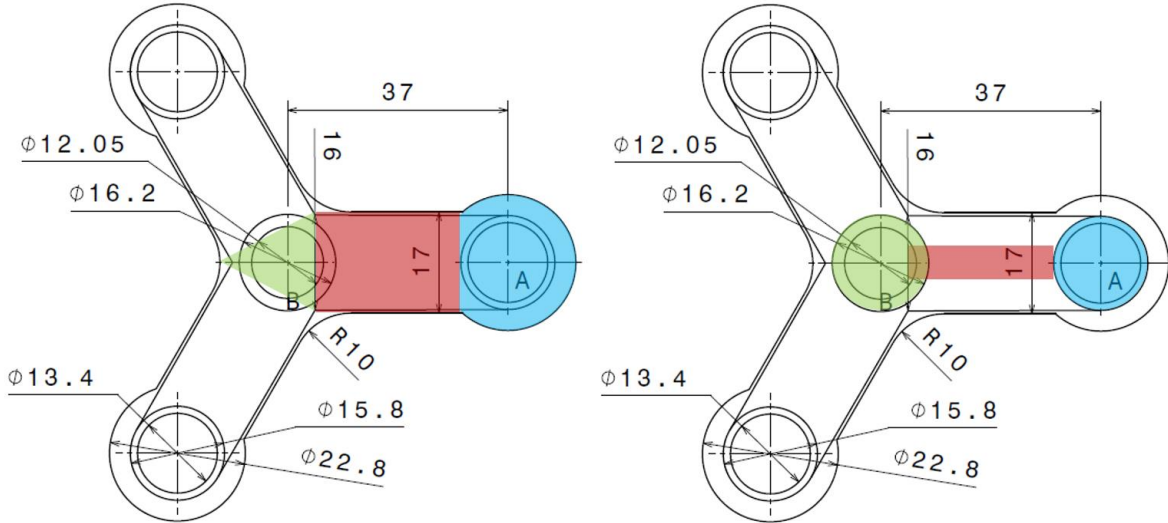


Figure 8: Physical (left) and model (right) representations of the star-shaped pontoon and slab for the OO-Star Semi floating substructure

Outer heave plates (blue)

The heave plate drag coefficient C_{DHP} is taken as 10 from [17], as given in [1]. We note that the value is based on a model scale experiment where the Reynolds number is not identical to the full-scale value. On the other hand, the sharp edge geometry of heave plates is expected to lead to a smaller dependency of the drag coefficient on the Reynolds number. In the LIFES50+ project, physical model tests are carried out which further allows a determination of the floating substructures damping properties, yet still at model scale. As mentioned before, the axial loads at member ends in FAST are applied to the area of the corresponding member end, therefore the drag on the outer physical heave plate, with drag coefficient C_{DHP} and area A_{HP} , will be applied in the model with a drag coefficient $C_{DHP_{FAST}}$, scaled to the area of the bottom of the outer column, A_{col} . The resulting values are given in Table 8.

Pontoons (red)

The pontoon legs in FAST are defined as horizontal cylinders extending from a radial position r_1 of 4.62 m to a radial position r_2 of 29.10 m. This definition of pontoons leaves an “uncovered” central triangle, which is dealt with below. The transverse drag coefficient C_D is taken as 2.05 [1], due to flow separation at the sharp corners. Each physical leg cross-section can be simplified to a rectangle, with height h_1 of 7 m and width h_2 of 17 m (the slight tapering of the pontoons is neglected for simplicity). In FAST, each pontoon is modelled as a cylinder with diameter D equal to h_1 . This ensures that the drag in the surge/sway plane will be properly modelled.

Central heave plate (green)

Since the pontoon leg width is more than twice the pontoon height, the drag loads on the legs in heave and pitch DoFs would be underestimated. To compensate for that, the missing drag is lumped into the three outer heave plates and a central, virtual heave plate (see Figure 8), which also captures the drag on the green triangle not covered by the pontoon.



To determine the drag coefficients of these heave plates (labelled as $C_{DHP0_{FAST}}$ for the central heave plate and $C_{DHP_{FAST}}$ for the outer heave plates), a set of equations was solved. In Eq. (9), the physical (left-hand side) drag force in heave on one leg of the real structure is equal to the heave force seen by the FAST model (right-hand side). In a similar manner, Eq. (10) relates the physical drag moment in pitch on one leg to the one seen by the model:

$$\begin{aligned} & \int_{r_1}^{r_2} \frac{1}{2} \rho C_D h_2 \dot{z} |\dot{z}| dr + \frac{1}{2} \rho C_{DHP} A_{HP} \dot{z} |\dot{z}| + \frac{1}{3} \frac{1}{2} \rho C_D A_{tri} \dot{z} |\dot{z}| \\ &= \int_{r_1}^{r_2} \frac{1}{2} \rho C_D D \dot{z} |\dot{z}| dr + \frac{1}{4} \rho C_{DHP_{FAST}} A_{col} \dot{z} |\dot{z}| + \frac{1}{3} \frac{1}{4} \rho C_{DHP0_{FAST}} A_{col0} \dot{z} |\dot{z}| \end{aligned} \quad (9)$$

$$\begin{aligned} & \int_{r_1}^{r_2} \frac{1}{2} \rho C_D h_2 \dot{\theta} |\dot{\theta}| r^3 dr + \frac{1}{2} \rho C_{DHP} A_{HP} \dot{\theta} |\dot{\theta}| R^3 \\ &= \int_{r_1}^{r_2} \frac{1}{2} \rho C_D D \dot{\theta} |\dot{\theta}| r^3 dr + \frac{1}{4} \rho C_{DHP_{FAST}} A_{col} \dot{\theta} |\dot{\theta}| R^3 \end{aligned} \quad (10)$$

Here r is the radial coordinate measured from the centre of the floating substructure, \dot{z} is the heave velocity, $\dot{\theta}$ is the pitch velocity, A_{tri} is the triangular area and A_{col} is the area of the bottom of the central column. The last term on the left-hand side of Eq. (9) is the drag on the central triangle, while the last term on the right-hand side is the contribution from the virtual central heave plate, necessary to correctly model the drag in the heave direction. For simplicity, only drag due to floating substructure motion is considered in Eqs. (9) and (10), i.e. no wave kinematics were included. Also, the contribution of the central triangle to Eq. (10) was neglected. The two equations were solved simultaneously to yield values of 38.34 for $C_{DHP_{FAST}}$ and 14.99 for $C_{DHP0_{FAST}}$. This axial drag coefficients are doubled, because only one joint per heave plate was employed here, contrary to HydroDyn's assumption of two joints per heave plate. A summary of the physical and model properties involved in the viscous drag on the bottom pontoon and slab of the OO-Star Semi floating substructure is given in Table 8.

Table 8: Summary of drag properties for bottom slab of OO-Star Semi floating substructure. The values on the right column have been determined to match the global drag in surge, heave and pitch for the physical structure

Property	Physical value	Model value	Colour in Figure 8
Pontoon leg height	7 m	7 m (diameter)	Red
Pontoon leg width	17 m	7 m (diameter)	Red
Transversal drag coefficient for pontoon	2.05	2.05	Red
Outer heave plate area	368.57 m ²	196.07 m ²	Blue
Outer heave plate drag coefficient	10	38.34	Blue
Central heave plate area	125.14 m ² (triangle)	206.12 m ²	Green
Central heave plate drag coefficient	2.05	14.99	Green



5.4 System identification

5.4.1 Static equilibrium

A first simulation with no wind, no waves and no initial displacements is run to assess model stability and correct balance between gravitational and buoyancy forces. Due to imperfect balance between global mass and net buoyancy, and to the tower-top CM not being aligned with the tower axis, a small offset is observed in surge, heave and pitch (see Table 9). This offset is used as initial condition in all the simulations to reduce the transient time.

Table 9: Static offset in FAST for the OO-Star Semi

Surge offset	Heave offset	Pitch offset
[m]	[m]	[deg]
0.1121	0.0540	-0.2328

5.4.2 Free decays

Free decay simulations have been carried out in the OO-Star Semi FAST model, where for each decay case, an initial displacement is introduced in the corresponding DoF and the system is left to decay to its equilibrium position (see Figure 9). A Fourier analysis of the relevant time series reveals the natural frequencies involved, as well as couplings between DoFs and the level of damping. The initial displacement chosen is representative of the given DoF. The tower decay is carried out with all turbine and floating substructure DoFs active. The natural frequencies are presented in Table 10.

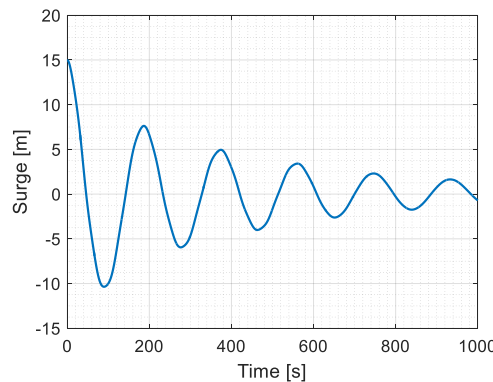


Figure 9: Time series of surge free decay for the OO-Star Semi

Table 10: System natural frequencies from FAST decay simulations for the OO-Star Semi

Surge	Heave	Pitch	Yaw	Tower
[Hz]	[Hz]	[Hz]	[Hz]	[Hz]
0.0054	0.0478	0.0316	0.0097	0.746



5.4.3 Response to regular waves

The model response to a regular wave with no wind is useful to assess whether the hydrodynamics are properly modelled. The response of the OO-Star Semi FAST model to a regular wave with $H=6$ m and $T=10$ s is shown in Figure 10, where the first 1200 s have not been included in the power spectral density (PSD) analysis to discard transient effects. It is observed that the floating substructure motion is dominated by the wave frequency at 0.1 Hz.

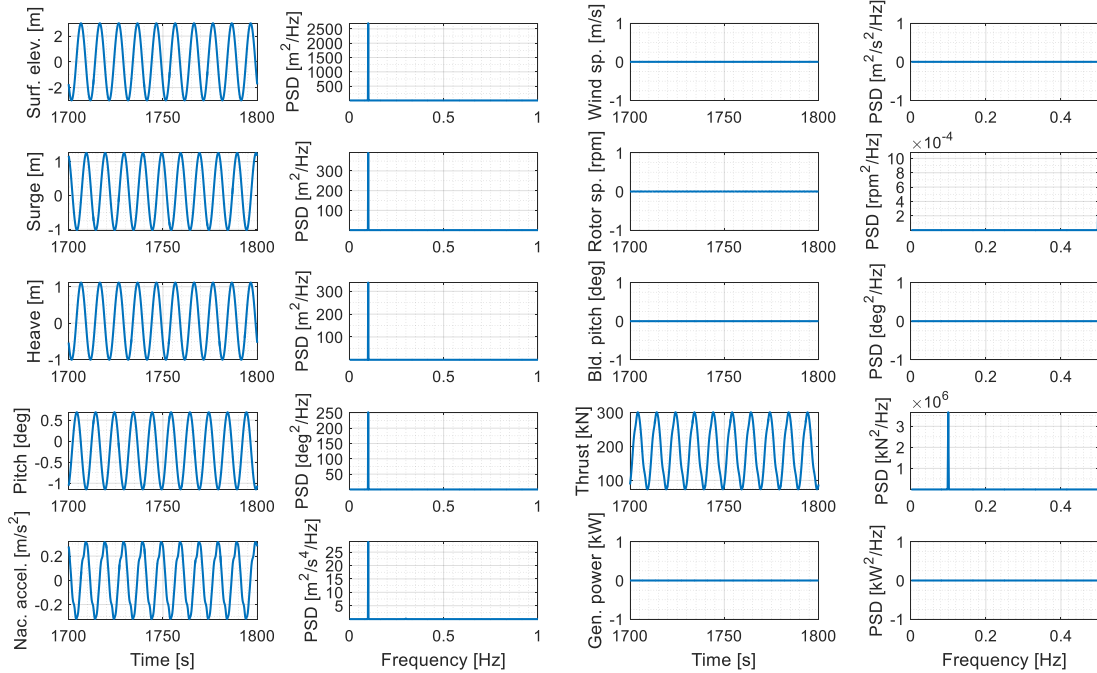


Figure 10: Response to regular waves for the OO-Star Semi

For the simulation with regular waves shown here, a strange behaviour was observed for the mooring line tension signals (see Figure 11). After 512 s, the amplitude of all mooring tensions is significantly increased over one-time step. The floating substructure motion signals, however, do not show this effect. The cause of this behaviour is still unknown and is currently under investigation together with the developer of MoorDyn.

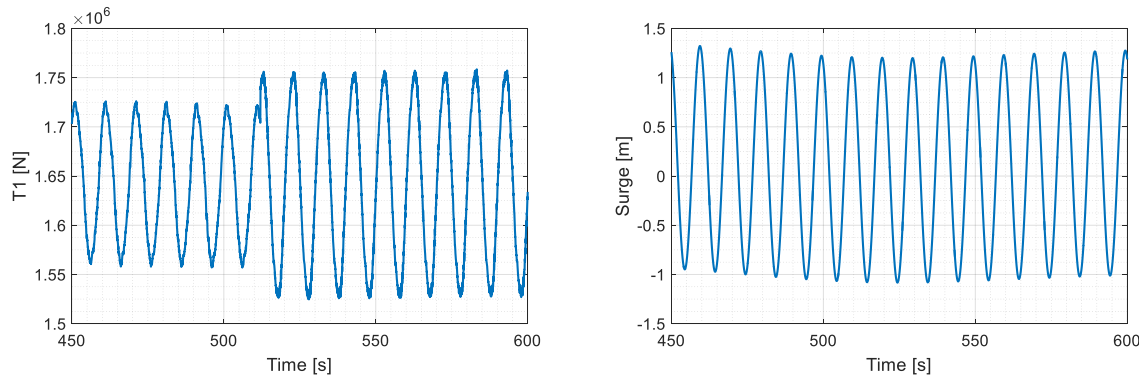


Figure 11: Mooring tension and floater surge in regular waves for the OO-Star Semi



5.4.4 Response to step uniform wind

The controller can be tested by simulating a case with no waves and uniform, steady wind speed that goes from cut-in wind speed 4 m/s to cut-out 25 m/s, changing in intervals of 1 m/s every 10 min (see Figure 12, where the first 1800 s have been excluded).

Every time the wind speed is increased, the thrust on the rotor changes and the floating substructure moves to its new equilibrium position, describing oscillations around it that decay with time. These oscillations happen at the natural frequency in each DoF. Because of the long surge natural period, the structure is still oscillating in surge when the wind speed is changed again. An important observation here is that the surge motion seems to be less damped for wind speeds between 11.4 and 16 m/s, although the controller was tuned to provide positive damping in floating substructure pitch in the full-load region. Further investigations revealed that, due to the controller, the aerodynamic damping in surge is negative or zero for these wind speeds. However, in real environmental conditions (i.e. wind and waves), we observed that the hydrodynamic damping contributes to a positive global damping of the surge mode. In the case shown in Figure 12, since no waves are present, the effect of the aerodynamic damping in surge is more visible. This controller effect is similar to the negatively-damped pitch motion reported in [4]. A solution similar to the one proposed in [4] would entail tuning the controller so its natural frequency is below the floating substructure's surge natural frequency. This approach, however, would significantly affect the wind turbine power production. Since the surge global damping has been observed to be positive in real-life environmental conditions due to hydrodynamic effects, this action is not recommended. Exploitation of further control strategies can likely lead to improved performance and is left for future work.

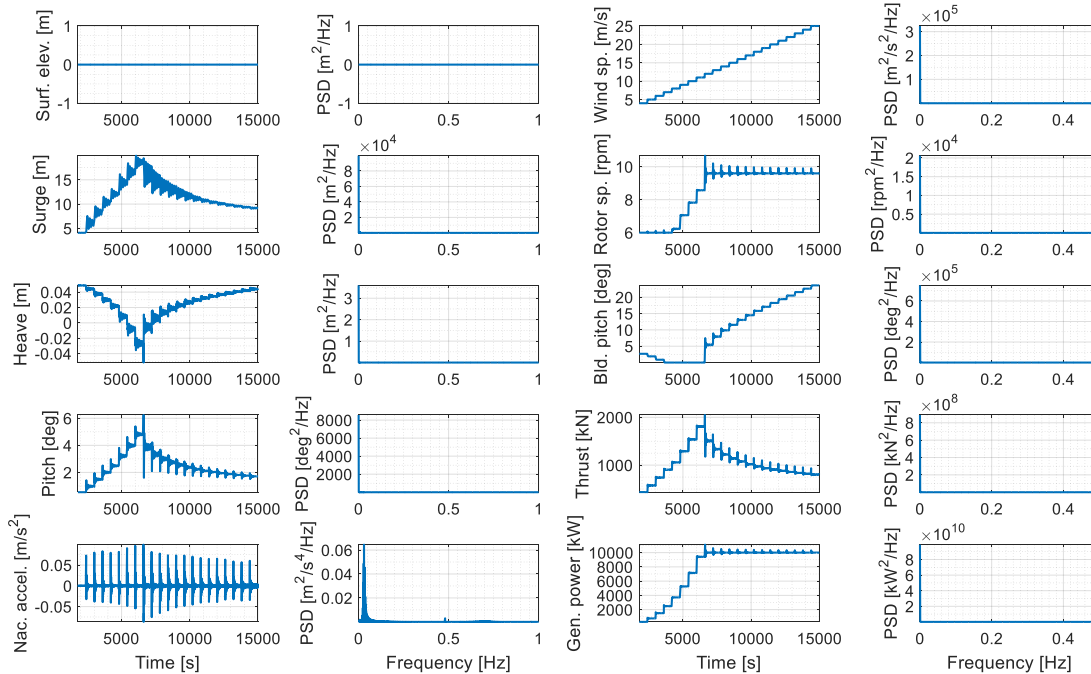


Figure 12: Response to step uniform wind for the OO-Star Semi



5.5 Response to wind and waves

5.5.1 Operational conditions

Figure 13 below show the response to irregular waves and turbulent wind in operational conditions. The load case is #12 in Table 1, with $V = 13.9 \text{ m/s}$, $H_s = 3.04 \text{ m}$ and $T_p = 9.5 \text{ s}$. The first 1800 s have been excluded from the PSD analysis to discard transient effects.

The surge and pitch motions are dominated by the surge and pitch natural frequencies respectively, likely excited by the wind forcing. The heave motion, on the other hand, is dominated by wave forcing. The nacelle acceleration shows response at the wave frequency range and at the tower natural frequency, although the response at the tower frequency is significantly lower. The turbine operates as expected with respect to rotor speed, blade pitch and generator power.

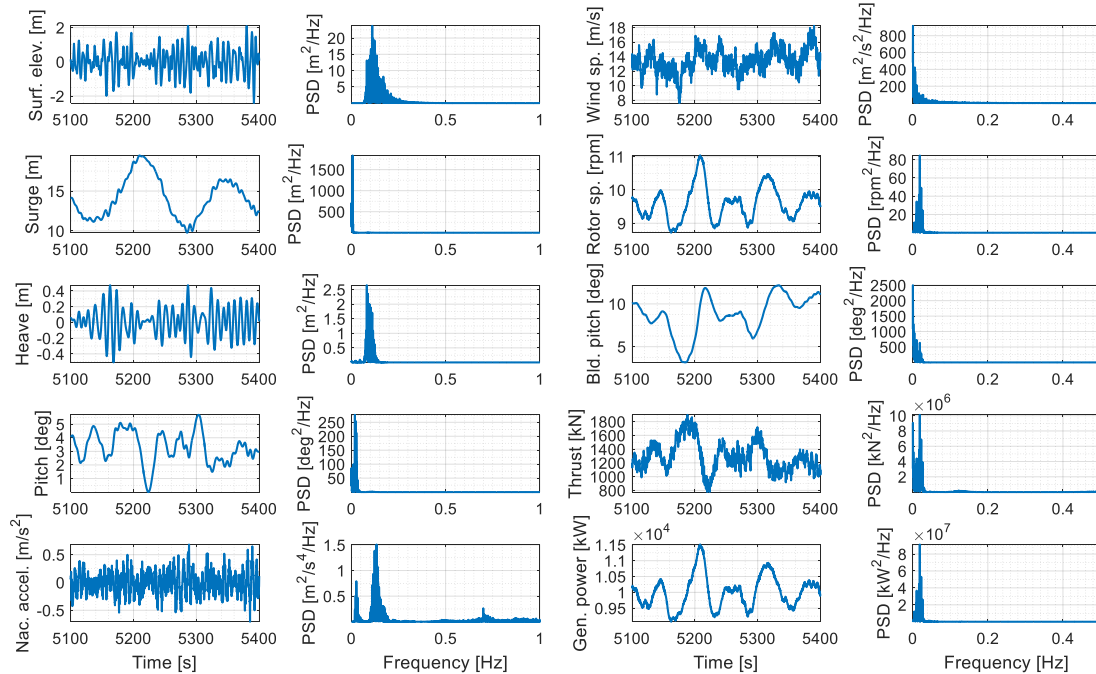


Figure 13: Response to load case #12 for the OO-Star Semi



5.5.2 Ultimate conditions

Figure 14 below shows the response to irregular waves and turbulent wind in ultimate conditions. The load case is #17 in Table 1, with $V = 22.1 \text{ m/s}$, $H_s = 10.9 \text{ m}$ and $T_p = 16 \text{ s}$ (50-year design wave). The first 1800 s have been excluded from the PSD analysis.

In this case the wave forcing dominates most of the floating substructure motions, although the wind forcing also seems to excite the natural frequencies of the surge and pitch modes. As in the case presented in Section 5.5.1 above, the PSD of nacelle acceleration shows some minor energy at the coupled tower natural frequency. Once again, the turbine operates normally in terms of rotor speed, blade pitch and generator power.

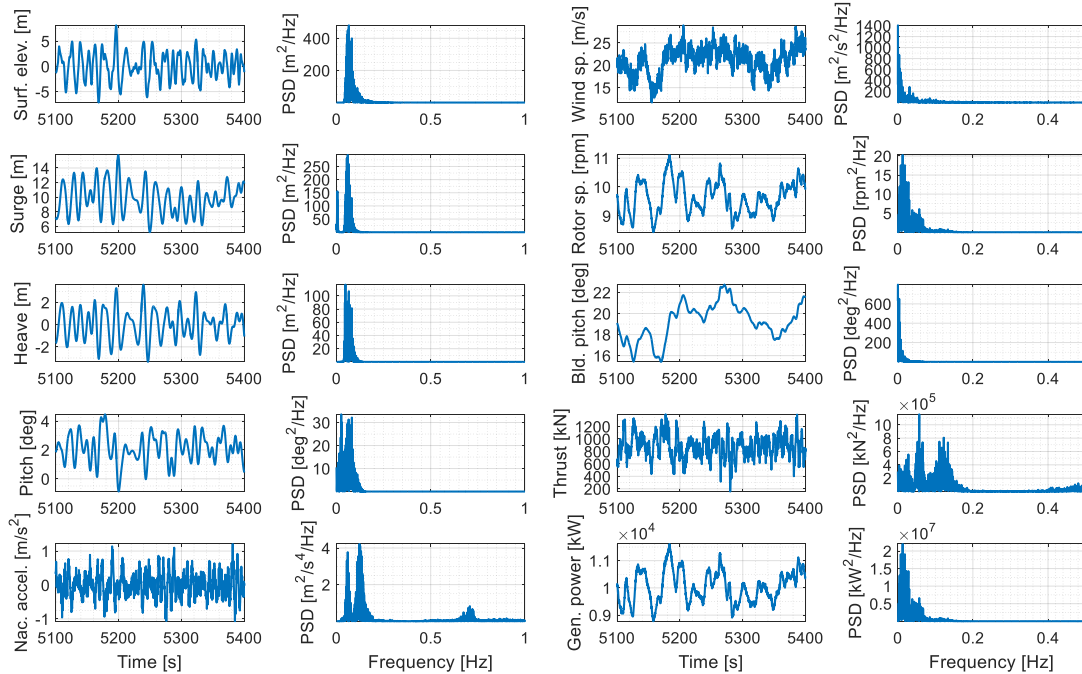


Figure 14: Response to load case #17 for the OO-Star Semi

5.5.3 Extreme conditions

Figure 15 below show the response to irregular waves and turbulent wind in extreme conditions. The load case is #18 in Table 1, with $V = 44$ m/s, $H_s = 10.9$ m and $T_p = 16$ s. The first 1800 s have been excluded from the PSD analysis to discard transient effects.

The difference between this case and the one presented above is that the wind speed is here 44 m/s and therefore the turbine is parked, with the blades in feather position. The responses are solely wave dominated in this case, given that the aerodynamic forces on the rotor are significantly smaller, and drag loads on the tower are not included. However, some wind-induced surge motion can still be observed. The response of the nacelle at the coupled tower frequency is not present anymore, which indicates it was due to the wind.

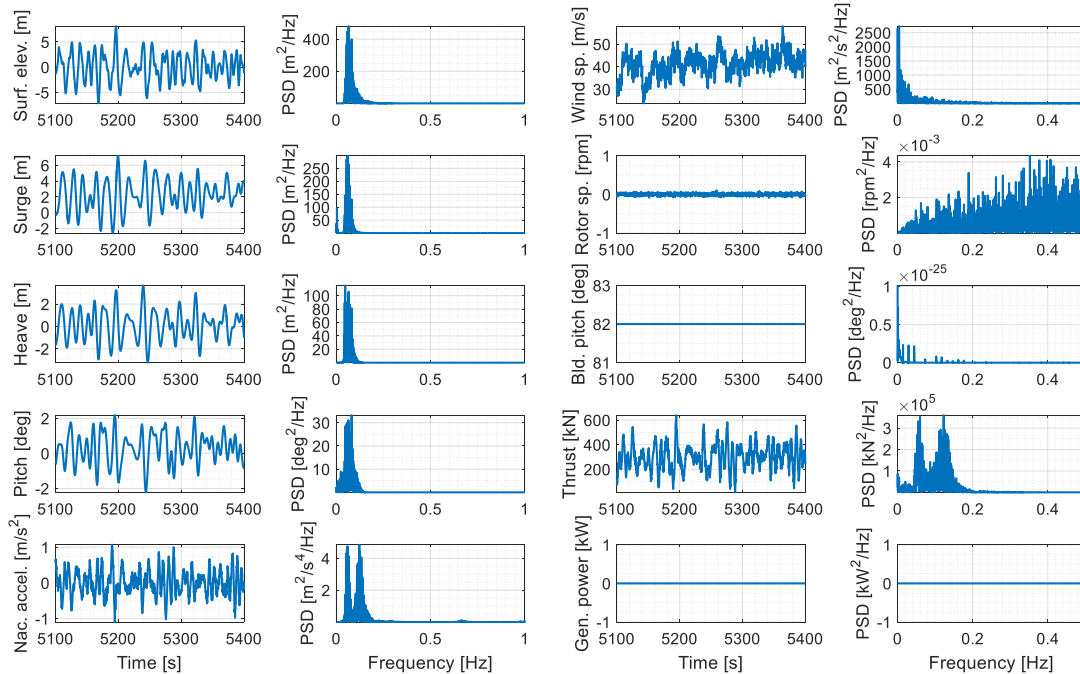


Figure 15: Response to load case #18 for the OO-Star Semi



6 Numerical model of the NAUTILUS-DTU10 floating wind turbine

The NAUTILUS-10 floating substructure (see Figure 16) is extensively described in [1] and [7]. Some of the main properties are collected in Table 11 below. For brevity, through this report sometimes the NAUTILUS-10 floating substructure will be referred to as “NAUTILUS-10”, whereas “NAUTILUS-DTU10” refers to the floating substructure together with the DTU 10MW RWT.

Table 11: Main properties of the NAUTILUS-10 floating substructure considering fully loaded tanks

Type	Material	Draft	Freeboard	Displaced volume	Floating substructure mass
		[m]	[m]	[m ³]	[kg]
Semisubmersible	Structural steel, concrete (passive ballast) and sea water (active ballast)	18.33	7.67	9.2810E+03	7.781E+06



Figure 16: The NAUTILUS-DTU10 floating wind turbine. Figure provided by Nautilus Floating Solutions SL [7]

6.1 Modelling of the tower

The *semi-flexible* approach presented in Section 5.1 for the modelling of the tower was not applied to the tower of the NAUTILUS-10 floating substructure due to the deck-type connection between tower



base and floater columns. Instead, the turbine configuration was modelled with the traditional *rigid* approach (i.e. flexible tower defined from nacelle to the interface between the tower and the floating sub-structure).

6.2 Modelling of the mooring system

The mooring line properties for the NAUTILUS-10 floating substructure are defined in [1]. In the FAST model, one catenary mooring line is defined between each AP and FLP, as summarized in Table 12 below.

Table 12: Mooring lines for the NAUTILUS-10 floating substructure

Line #	Anchor coordinates			Fairlead coordinates		
	X	Y	Z	X	Y	Z
	[m]	[m]	[m]	[m]	[m]	[m]
1	592.18	592.18	-130.00	31.09	31.09	-6.33
2	-592.18	592.18	-130.00	-31.09	31.09	-6.33
3	-592.18	-592.18	-130.00	-31.09	-31.09	-6.33
4	592.18	-592.18	-130.00	31.09	-31.09	-6.33

The mooring lines are studless chains with an unstretched length of 833.24 m each. In the FAST model, each line was discretized into 100 segments. The line internal damping ratio was set to 1, as recommended in the MoorDyn User's Guide [14].

6.3 Modelling of the hydrodynamics

6.3.1 First-order radiation-diffraction hydrodynamics

The hydrostatic restoring matrix, referred to the centre of flotation and assuming centred CM of the rotor-nacelle assembly, is presented in Table 13. It can be observed that, due to the floating substructure's symmetry, only the diagonal elements corresponding to heave, roll and pitch are non-zero, and the roll and pitch diagonal elements are identical. The hydrostatic matrix shown here was computed in WAMIT and only includes the effects of water plane area and buoyancy, since the mass contributions are internally computed by FAST.

Table 13: Hydrostatic restoring matrix for the NAUTILUS-10 floating substructure considering fully loaded tanks

	1 (Surge)	2 (Sway)	3 (Heave)	4 (Roll)	5 (Pitch)	6 (Yaw)
1 (Surge)	0	0	0	0	0	0
2 (Sway)	0	0	0	0	0	0
3 (Heave)	0	0	3.4511E+06	0	0	0
4 (Roll)	0	0	0	1.5170E+09	0	0
5 (Pitch)	0	0	0	0	1.5170E+09	0
6 (Yaw)	0	0	0	0	0	0



The added mass, radiation damping and wave diffraction forces (for zero degrees wave heading) for the NAUTILUS-10 floating substructure computed using WAMIT are shown in Figure 17, Figure 18 and Figure 19, respectively.

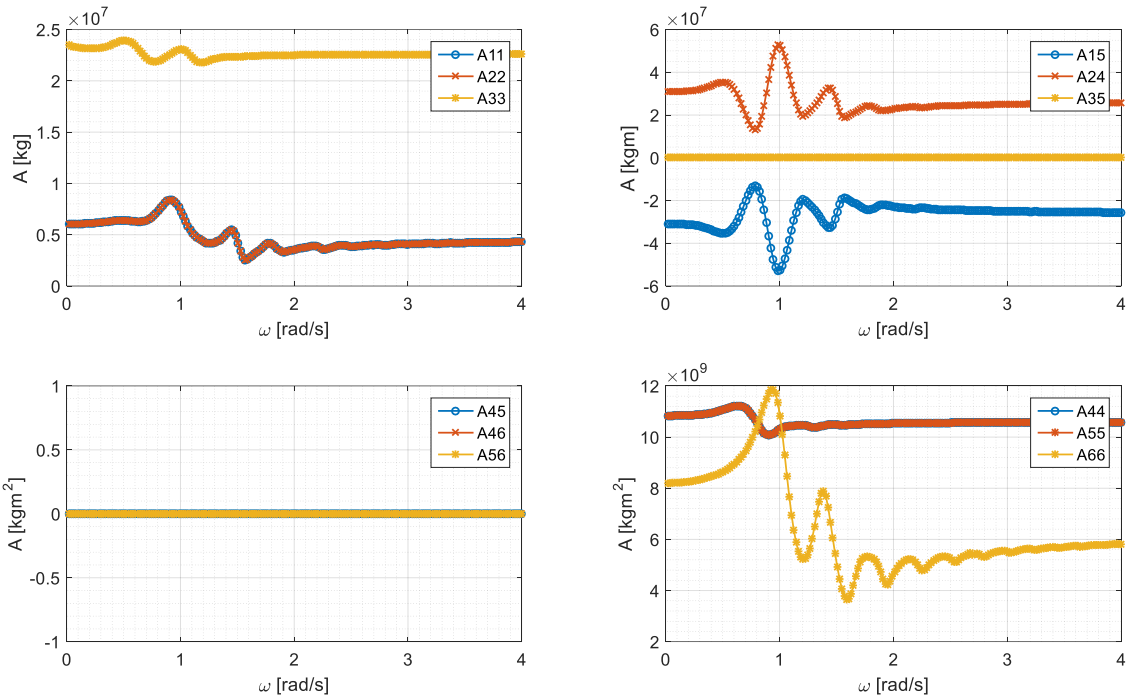


Figure 17: Added mass for the NAUTILUS-10 floating substructure considering fully loaded tanks

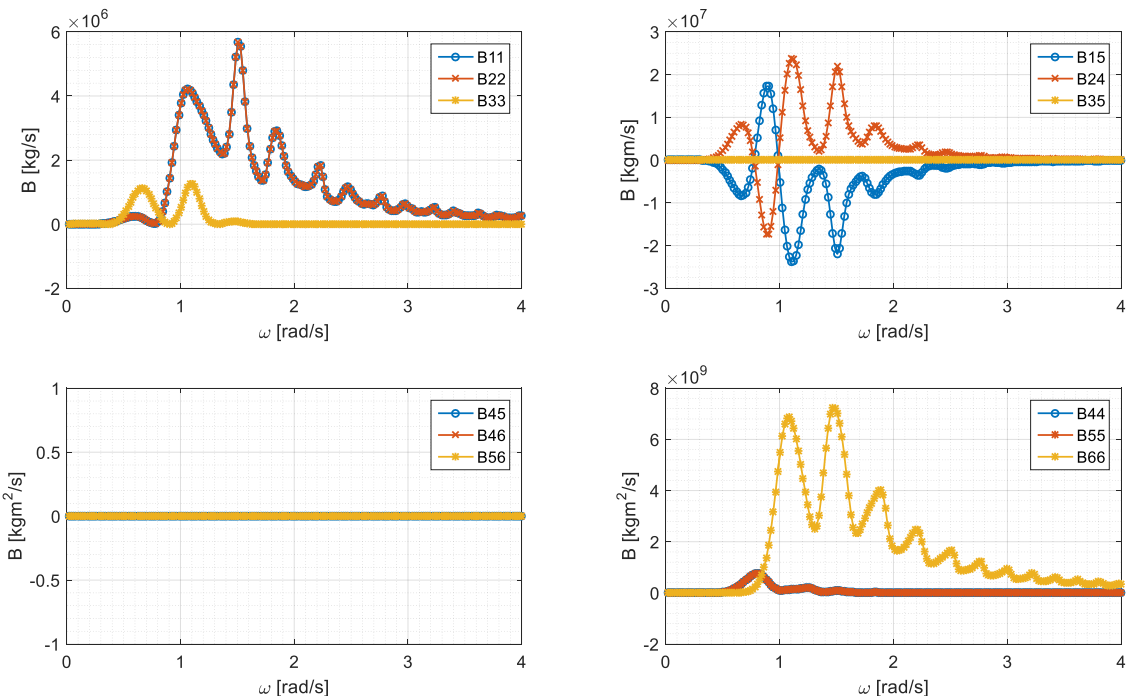


Figure 18: Radiation damping for the NAUTILUS-10 floating substructure considering fully loaded tanks



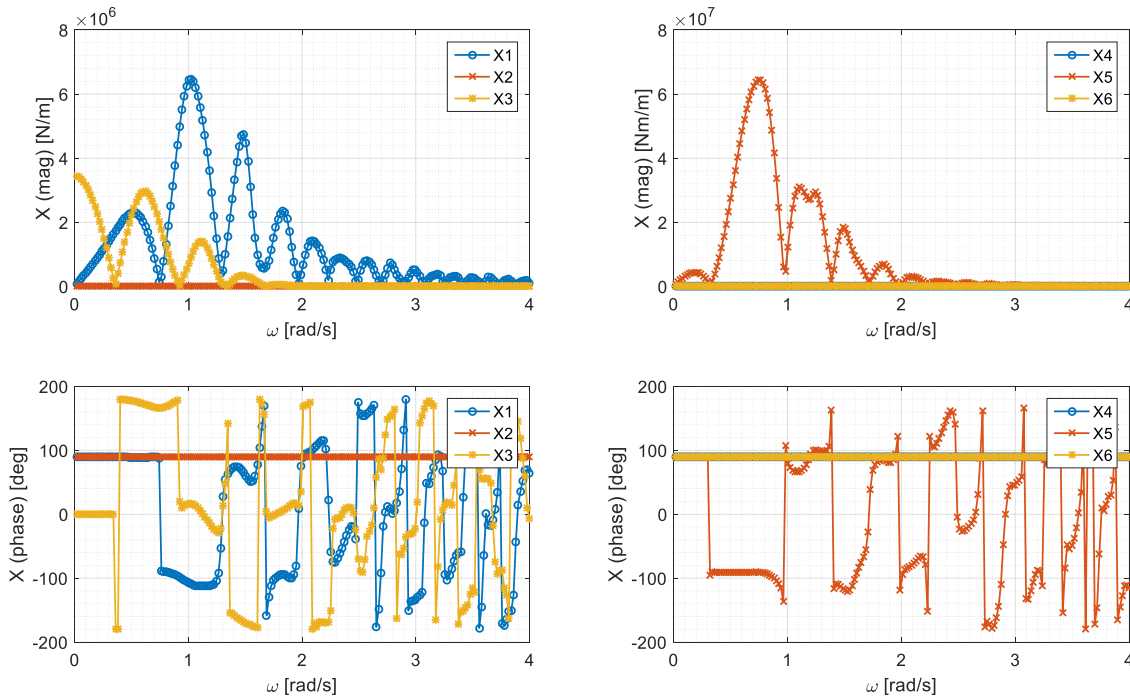


Figure 19: Wave diffraction forces for the NAUTILUS-10 floating substructure considering fully loaded tanks, magnitude (top) and phase (bottom)

The NAUTILUS-10 floating substructure employs an active ballast system to counteract the overturning moment from the wind (see [1] and [7]). The active ballast system modifies the floating substructure mass, center of mass and mass moment of inertia according to the mean wind speed and direction, among other parameters. Thus, it also has an effect on the draft of the NAUTILUS-DTU10 floating wind turbine, with draft differences of 1.5 m between cut-in and rated wind speeds (as reported in [7]). In the NAUTILUS-DTU10 FAST model, the floating substructure mass, center of mass and moments of inertia in the ElastoDyn input file are updated accordingly for each simulation based on the mean wind speed, according to Table 18 of [1] (further information can be found in [7]). Ideally, one would also use case-dependent WAMIT data and displaced water volume for each environmental condition, taking into account the real draft for each case. Here, however, a simpler approach was chosen, and all the simulations were carried out using the WAMIT data and the displaced water volume corresponding to the no-wind ballasting condition (fully loaded tanks). This approach, although simpler, is consistent with the statement in Section 3.1.3 and between the two floating substructures considered in this document. No comparison between the modelling approach taken here and the case-dependent hydrodynamic properties has been made.

6.3.2 Viscous effects

To capture viscous effects in the NAUTILUS-10 floating substructure, linear and quadratic damping matrices lumped at the centre of flotation have been included in the FAST model, with the values given in Table 14. These matrices were obtained by Nautilus Floating Solutions SL from earlier model-scale experiments [1] [7] and will be updated once the tests for the NAUTILUS-DTU10 floating wind turbine are carried out within LIFES50+. This modelling approach only considers the floating substructure global velocity instead of the relative velocity between the floating substructure and the wave field, hence it only covers the damping part of the Morison drag formulation and neglects the viscous forcing part (see Eq. (2)). An alternative Morison-based formulation of the viscous effects on the NAUTILUS-10 floating substructure can be seen in the Appendix.



Table 14: Linear and quadratic hydrodynamic viscous damping matrices for the NAUTILUS-10 floating substructure [1] [7]

Linear	1 (Surge)	2 (Sway)	3 (Heave)	4 (Roll)	5 (Pitch)	6 (Yaw)
1 (Surge)	0	0	0	0	0	0
2 (Sway)	0	0	0	0	0	0
3 (Heave)	0	0	3.3548E+05	0	0	0
4 (Roll)	0	0	0	2.1197E+08	0	0
5 (Pitch)	0	0	0	0	2.2217E+08	0
6 (Yaw)	0	0	0	0	0	2.2560E+07
Quadratic						
1 (Surge)	1.1010E+06	0	0	0	0	0
2 (Sway)	0	8.2731E+05	0	0	0	0
3 (Heave)	0	0	5.6380E+06	0	0	0
4 (Roll)	0	0	0	3.8515E+10	0	0
5 (Pitch)	0	0	0	0	4.1618E+10	0
6 (Yaw)	0	0	0	0	0	7.0665E+09



6.4 System identification

6.4.1 Static equilibrium

A first simulation with no wind, no waves and no initial displacements is run to assess model stability and correct balance between gravitational and buoyancy forces. Due to imperfect balance between global mass and net buoyancy, and to the tower-top CM not being aligned with the tower axis, a small offset is observed in surge, heave and pitch (see Table 15). This offset is used as initial condition in all the simulations to reduce the transient time.

Table 15: Static offset in FAST for the NAUTILUS-DTU10

Surge offset	Heave offset	Pitch offset
[m]	[m]	[deg]
0.0576	-0.0453	-0.2441

6.4.2 Free decays

Free decay simulations have been carried out in the NAUTILUS-DTU10 FAST model, where for each decay case, an initial displacement is introduced in the corresponding DoF and the system is left to decay to its equilibrium position (see Figure 20). A Fourier analysis of the relevant time series reveals the natural frequencies involved, as well as couplings between DoFs and the level of damping. The initial displacement chosen is representative of the given DoF. The tower decay is carried out with all turbine and floating substructure DoFs active. The natural frequencies are presented in Table 16.

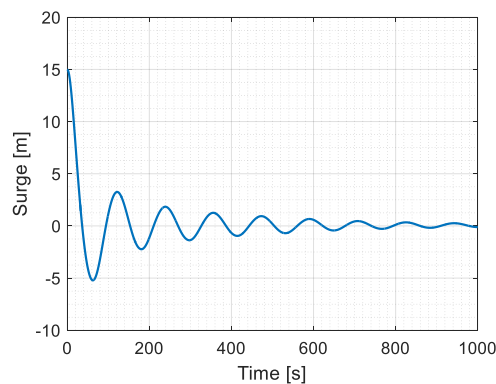


Figure 20: Time series of surge free decay for the NAUTILUS-DTU10

Table 16: System natural frequencies from FAST decay simulations for the NAUTILUS-DTU10

Surge	Heave	Pitch	Yaw	Tower
[Hz]	[Hz]	[Hz]	[Hz]	[Hz]
0.0085	0.0518	0.0340	0.0107	0.526



6.4.3 Response to regular waves

The model response to a regular wave with no wind is useful to assess whether the hydrodynamics are properly modelled. The response of the NAUTILUS-DTU10 FAST model to a regular wave with $H=6$ m and $T=10$ s is shown in Figure 21, where the first 1200 s have not been included in the power spectral density (PSD) analysis to discard transient effects. It is observed that the floating substructure motion is dominated by the wave frequency at 0.1 Hz.

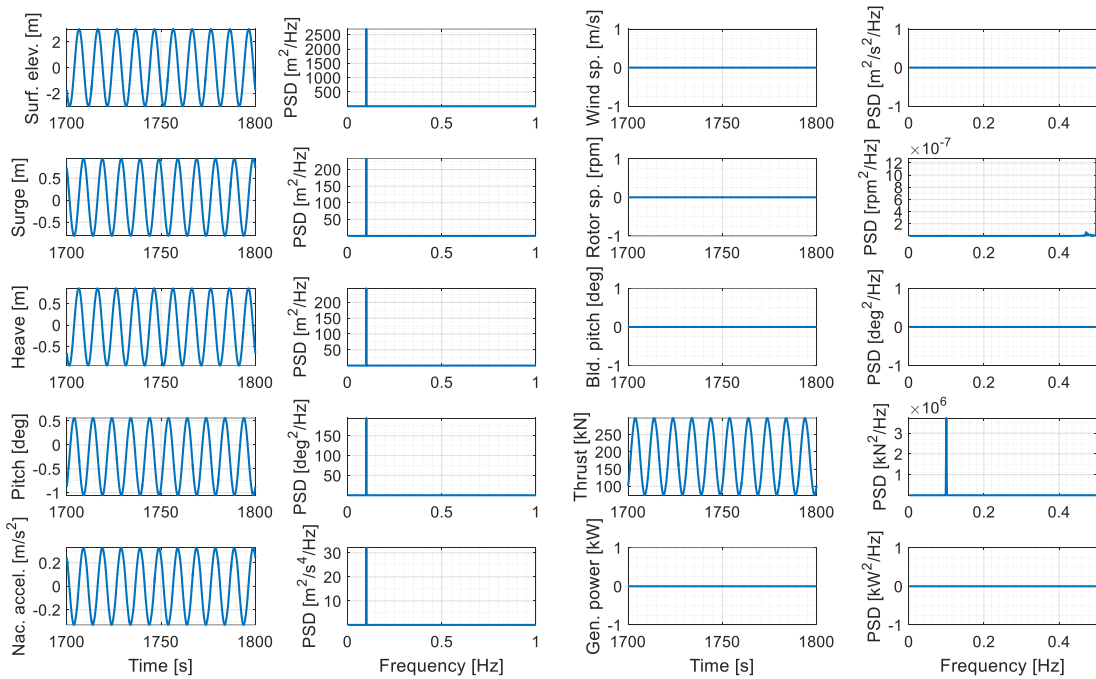


Figure 21: Response to regular waves for the NAUTILUS-DTU10

For the simulation with regular waves shown here, a strange behaviour was observed for the mooring line tension signals (see Figure 22). After 512 s, the amplitude of all mooring tensions is significantly increased over one-time step. The floating substructure motion signals, however, do not show this effect. The cause of this behaviour is still unknown and is currently under investigation together with the developer of MoorDyn.

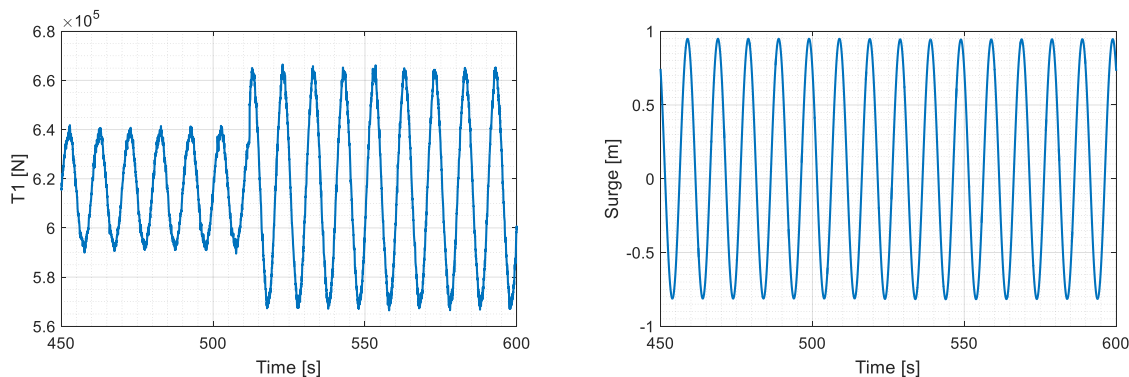


Figure 22: Mooring tension and floater surge in regular waves for the NAUTILUS-DTU10

6.4.4 Response to step uniform wind

The controller can be tested by simulating a case with no waves and uniform, steady wind speed that goes from cut-in wind speed 4 m/s to cut-out 25 m/s, changing in intervals of 1 m/s every 10 min (see Figure 23, where the first 1800 s have been excluded). The reader should note that the active ballast system of the NAUTILUS-10 floating substructure is not active here, given that the floating substructure properties cannot be dynamically changed within the simulation. Instead, the floating substructure is fully ballasted as for the cases with no wind.

Every time the wind speed is increased, the thrust on the rotor changes and the floating substructure moves to its new equilibrium position, describing oscillations around it that decay with time. These oscillations happen at the natural frequency in each DoF. Because of the long surge natural period, the structure is still oscillating in surge when the wind speed is changed again. An important observation here is that the surge motion seems to be less damped for wind speeds between 11.4 and 16 m/s, although the controller was tuned to provide positive damping in floating substructure pitch in the full-load region. Further investigations revealed that, due to the controller, the aerodynamic damping in surge is negative or zero for these wind speeds. However, in real environmental conditions (i.e. wind and waves), we observed that the hydrodynamic damping contributes to a positive global damping of the surge mode. In the case shown in Figure 23, since no waves are present, the effect of the aerodynamic damping in surge is more visible. This controller effect is similar to the negatively-damped pitch motion reported in [4]. A solution similar to the one proposed in [4] would entail tuning the controller so its natural frequency is below the floating substructure's surge natural frequency. This approach, however, would significantly affect the wind turbine power production. Since the surge global damping has been observed to be positive in real-life environmental conditions due to hydrodynamic effects, this action is not recommended. Exploitation of further control strategies can likely lead to improved performance and is left for future work.

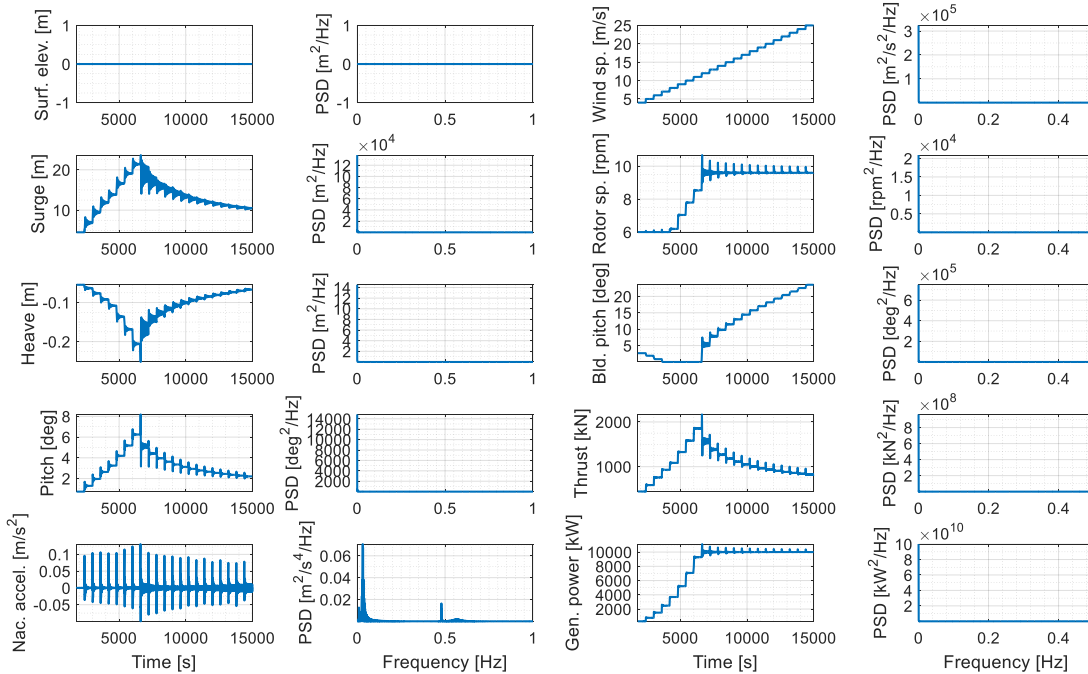


Figure 23: Response to step uniform wind for the NAUTILUS-DTU10



6.5 Response to wind and waves

6.5.1 Operational conditions

Figure 24 below shows the response to irregular waves and turbulent wind in operational conditions. The load case is #12 in Table 1, with $V = 13.9$ m/s, $H_s = 3.04$ m and $T_p = 9.5$ s. The first 1800 s have been excluded from the PSD analysis to discard transient effects.

The surge and pitch motions are dominated by the surge and pitch natural frequencies respectively, likely excited by the wind forcing. The heave motion, on the other hand, is dominated by wave forcing. The heave offset observed is due to the modelling choice mentioned in Section 3.1.3. Since the displaced water volume used in the simulation is that of the fully-ballasted case, but the mass of the floating substructure reflects the actual ballasting condition, the balance between buoyancy and gravity forces is found at a different draft. In other words, the heave signal given here is referred to the flotation point of the fully-ballasted case. The nacelle acceleration shows response at the wave frequency range and at the tower natural frequency. The turbine operates as expected with respect to rotor speed, blade pitch and generator power.

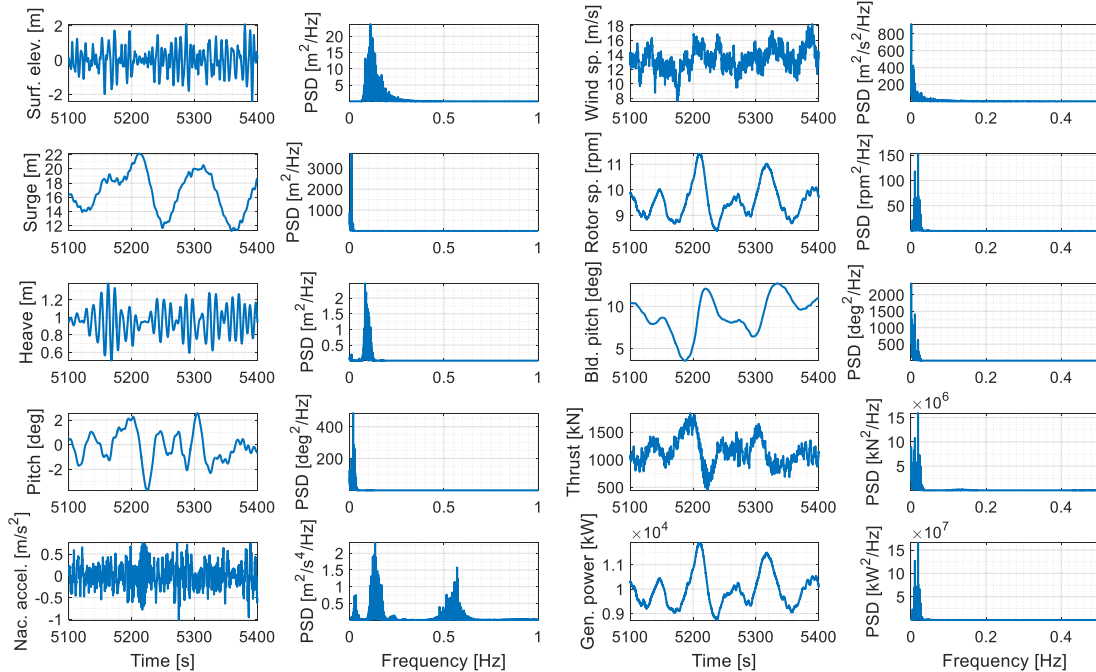


Figure 24: Response to load case #12 for the NAUTILUS-DTU10



6.5.2 Ultimate conditions

Figure 25 and below shows the response to irregular waves and turbulent wind in ultimate conditions. The load case is #17 in Table 1, with $V = 22.1 \text{ m/s}$, $H_s = 10.9 \text{ m}$ and $T_p = 16 \text{ s}$ (50-year design wave). The first 1800 s have been excluded from the PSD analysis.

In this case the wave forcing dominates most of the floating substructure motions, although the wind forcing also seems to excite the natural frequencies of the surge and pitch modes. As in the case presented in Section 6.5.1 above, the PSD of nacelle acceleration shows some energy at the coupled tower natural frequency. Once again, the turbine operates normally in terms of rotor speed, blade pitch and generator power.

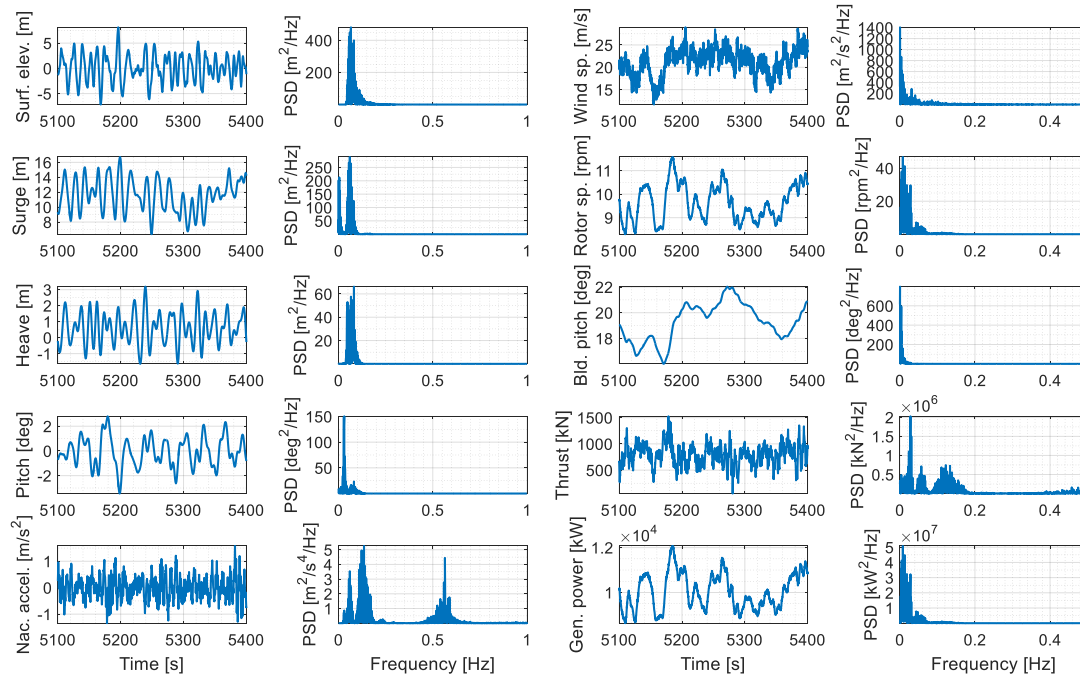


Figure 25: Response to load case #17 for the NAUTILUS-DTU10



6.5.3 Extreme conditions

Figure 26 below shows the response to irregular waves and turbulent wind in extreme conditions. The load case is #18 in Table 1, with $V = 44$ m/s, $H_s = 10.9$ m and $T_p = 16$ s. The first 1800 s have been excluded from the PSD analysis to discard transient effects.

The difference between this case and the one presented above is that the wind speed is here 44 m/s and therefore the turbine is parked, with the blades in feather position. The responses are solely wave dominated in this case, given that the aerodynamic forces on the rotor are significantly smaller, and drag loads on the tower are not included. However, some wind-induced surge motion can still be observed. The response of the nacelle at the coupled tower frequency is not present anymore, which indicates it was due to the wind.

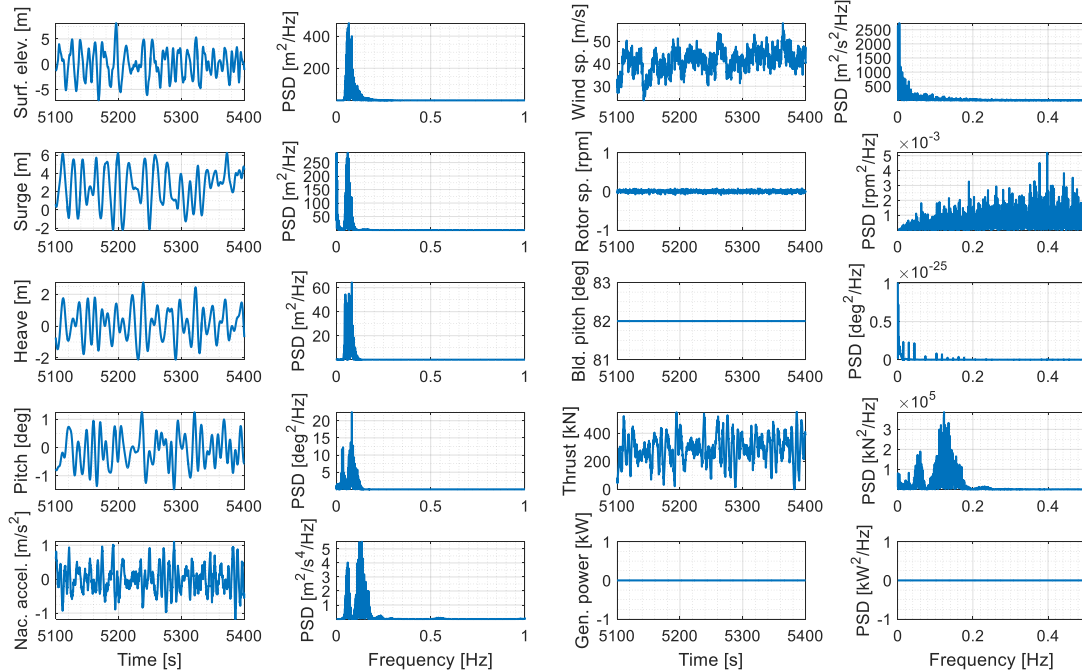


Figure 26: Response to load case #18 for the NAUTILUS-DTU10



7 Model accessibility and referencing

The two FAST models are freely available to the public from links at <http://dtu-10mw-rwt.vinden-ergi.dtu.dk/>. The NAUTILUS-DTU10 FAST model can also be downloaded from <https://www.researchgate.net/project/NAUTILUS-DTU10-MW-Floating-Offshore-Wind-Turbine-at-Gulf-of-Maine>.

In the event of publication of work resulting from the use of the OO-Star Semi FAST model, proper referencing to [18] should be included. If the NAUTILUS-DTU10 FAST model is used instead, [7] should be referenced. In all cases, appropriate referencing to [1] and the present report should be included.

8 Conclusions

We have presented the implementation in FAST of the DTU 10MW RWT mounted on two floating substructures, namely the LIFES50+ OO-Star Wind Floater Semi 10MW and the NAUTILUS-10 floating substructure. FAST v8.16.00a-bjj was selected as the version for developing the numerical model implementation. The wind turbine structural and aerodynamic models were already implemented in FAST within the LIFES50+ project. In this report, attention was given to the changes necessary to adapt the FAST model of the onshore DTU 10MW RWT to a floating foundation. These changes entail modelling of the tower, floating substructure hydrodynamics and mooring system, as well as tuning of the controller.

For each model, a first set of simulations for system identification purposes was carried out to assess system properties such as static offset, natural frequencies and response to regular waves. The controller was tested in simulations with uniform wind ranging from cut-in to cut-out wind speed. A set of simulations in stochastic wind and waves was carried out to characterize the global response of each floating substructure. The two FAST models presented in this report are available to the public as indicated above.



9 References

- [1] W. Yu, K. Müller and F. Lemmer, "LIFES50+ D4.2: Public definition of the two LIFES50+ 10MW floater concepts," University of Stuttgart, 2018.
- [2] M. Borg, M. Mirzaei and H. Bredmose, "LIFES50+ D1.2: Wind turbine models for the design," Technical University of Denmark, 2015.
- [3] C. Bak, F. Zahle, R. Bitsche, T. Kim, A. Yde, L. C. Henriksen, A. Natarajan and M. H. Hansen, "Description of the DTU 10MW Reference Wind Turbine," DTU Wind Energy Report I-0092, 2013.
- [4] T. J. Larsen and T. D. Hanson, "A method to avoid negative damped low frequent tower vibrations for a floating, pitch controlled wind turbine," *Journal of Physics: Conference Series*, vol. 75, 2007.
- [5] M. H. Hansen and L. C. Henriksen, "Basic DTU Wind Energy controller," DTU Wind Energy Report E-0028, 2013.
- [6] M. H. Hansen, A. Hansen, T. J. Larsen, S. Øye, P. Sørensen and P. Fuglsang, "Control design for a pitch-regulated, variable-speed wind turbine," Risø National Laboratory Technical Report Risø-R-1500(EN), 2005.
- [7] J. Galvan, M. Sanchez-Lara, I. Mendikoa, V. Nava, F. Boscolo-Papo, C. Garrido-Mendoza, J. Berque, G. Perez-Moran and R. Rodriguez-Arias, "Definition and analysis of NAUTILUS-DTU10 MW floating offshore wind turbine at Gulf of Maine, experiments at Sintef Ocean and Polimi," Tecnalia R&I, Derio, Basque Country, Spain, 2018.
- [8] J. Jonkman and B. Jonkman, "NWTC Information Portal (FAST v8)," National Renewable Energy Laboratory, 2016. [Online]. Available: <https://nwtc.nrel.gov/FAST8>. [Accessed 4 October 2017].
- [9] J. M. Jonkman, "Dynamics of Offshore Floating Wind Turbines - Model Development and Verification," *Wind Energy*, vol. 12, no. 5, pp. 459-492, 2009.
- [10] C. H. Lee and J. N. Newman, "WAMIT homepage," WAMIT, Inc., [Online]. Available: <http://www.wamit.com/index.htm>. [Accessed 4 October 2017].
- [11] W. E. Cummins, "The impulse response function and ship motions," *Schiffstechnik*, vol. 9, pp. 101-109, 1962.
- [12] J. N. Newman, *Marine Hydrodynamics*, Cambridge, MA: The MIT Press, 1997.
- [13] F. Wendt, A. Robertson, J. Jonkman and M. T. Andersen, "Verification and Validation of the New Dynamic Mooring Modules Available in FAST v8," in *Twenty-sixth (2016) International Ocean and Polar Engineering Conference (ISOPE)*, Rhodes, Greece, 2016.



- [14] M. Hall, "MoorDyn User's Guide," Department of Mechanical Engineering, University of Maine, 2015.
- [15] A. Krieger, G. K. V. Ramachandran, L. Vita, P. Gómez Alonso, G. González Almería, J. Berque and G. Aguirre, "LIFES50+ D7.2: Design basis," DNV-GL, 2015.
- [16] M. Borg, A. M. Hansen and H. Bredmose, "Floating substructure flexibility of large-volume 10MW offshore wind turbine platforms in dynamic calculations," *Journal of Physics: Conference Series*, vol. 753, no. 8, 2016.
- [17] L. Tao and D. Dray, "Hydrodynamic performance of solid and porous heave plates," *Ocean Engineering*, vol. 35, no. 10, pp. 1006-1014, 2008.
- [18] A. Pegalajar-Jurado, H. Bredmose, M. Borg, J. G. Straume, T. Landbø, H. S. Andersen, W. Yu, K. Müller and F. Lemmer, "State-of-the-art model for the LIFES50+ OO-Star Wind Floater Semi 10MW floating wind turbine," *Journal of Physics: Conference Series*, 2018.
- [19] J. Li, S. Liu and M. Zhao, "Experimental investigation of the hydrodynamic characteristics of heave plates using forced oscillation," *Ocean Engineering*, vol. 66, pp. 82-91, 2013.



10 Appendix

10.1 Inclusion of Morison drag in the LIFES50+ NAUTILUS-10 floating sub-structure

To model viscous drag on the NAUTILUS-10 floating substructure through the Morison equation, 9 members are defined as follows (see Figure 27):

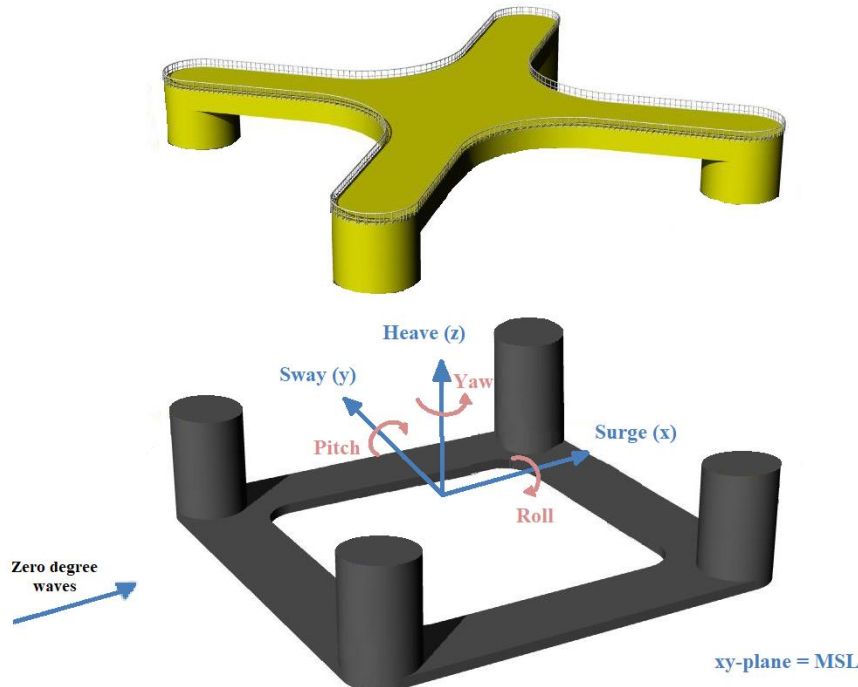


Figure 27: Geometry of the NAUTILUS-10 floating substructure [7], expanded view

- Four members represent the four vertical columns, with a transversal drag coefficient C_D of 0.715 [1] together with a physical diameter D_{col} of 10.5 m.
- Four members representing the square-shaped ring pontoon connecting the columns are defined to approximate the main drag loads on the pontoons. However, since FAST only allows the definition of cylindrical members, some modifications to the model representation are made. A sketch of the physical and the model representation of the square pontoon is presented in Figure 28. The properties of the members are described below and summarized in Table 17.
- The last member defined is a virtual thin heave plate with a diameter D_{col} of 10.5 m and a transversal drag coefficient C_D of 0 (i.e. this virtual member only contributes to the axial drag, not to the transversal drag). It is located at the same draft as the bottom of the columns, but in the centre of the floating substructure, i.e. $(x,y) = (0,0)$. The purpose of this member is to compensate for the missing drag force in heave when modelling the horizontal pontoons as cylindrical members, as detailed below.

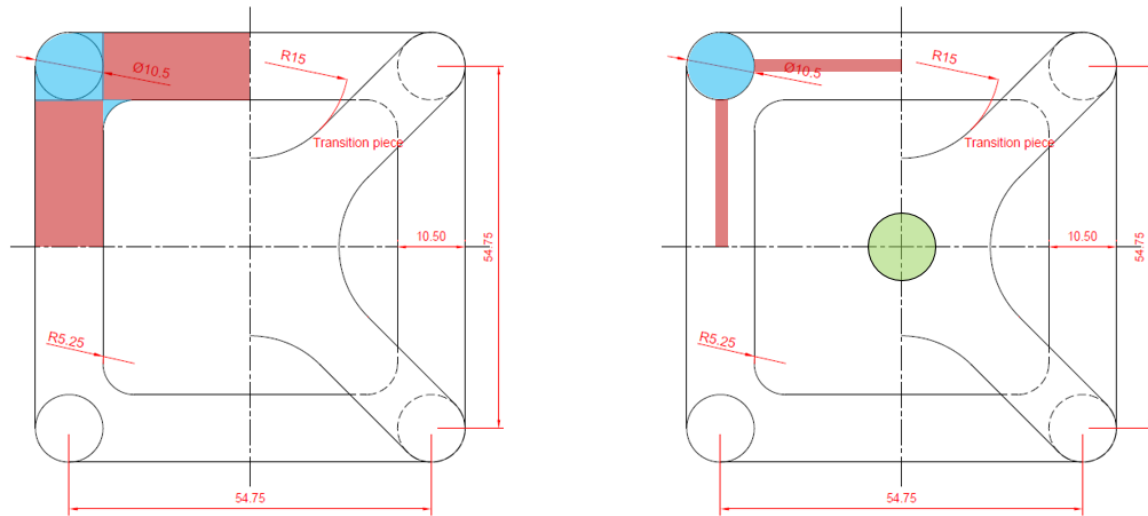


Figure 28: Physical (left) and model (right) representations of the pontoons for the NAUTILUS-10 floating substructure

Pontoons (red)

The pontoons are defined in FAST as cylinders extending from the circumference of the columns and along either the x- or y-axis up to the next column. The cylindrical members have a length L of 44.25 m and the transversal drag coefficient C_D is taken as 2.05 [1], due to flow separation at the sharp corners. This definition of pontoons leaves an “uncovered” area, which is dealt with below. In the physical structure the cross-section of the pontoons is a rectangle, with height h_1 of 1.5 m and width h_2 of 10.5 m. Since the members are required to be cylinders each pontoon is modelled with diameter D equal to h_1 , in order to ensure that the drag in the surge/sway plane will be properly modelled.

Outer heave plates (blue) and central heave plate (green)

Since the pontoon width h_2 is larger than the pontoon height h_1 , the drag loads in heave and pitch DoFs will be underestimated. To compensate for that, the missing drag loads are lumped into heave plates located under the vertical columns and a central, virtual heave plate (see Figure 28). The physical axial drag coefficient of the columns C_{Da} can be estimated by approximating the area under them to a square. From [19] the value for a square heave plate is taken as 7.12, but in order to compensate for the fact that only half of the edges are visible and that a long cylinder is present here instead of a heave plate, the value is reduced to $C_{Da} = \frac{1}{2} \frac{1}{2} 7.12 = 1.78$. As mentioned before, the axial loads at member ends in FAST are applied to the area of the corresponding member end, therefore the axial drag on the bottom of the column, with drag coefficient C_{Da} and area A_{square} , will be applied in the model with a drag coefficient $C_{Da_{FAST}}$, scaled to the area of the bottom of the column, A_{col} . To determine the axial drag coefficients in the model, a set of equations is solved (see below). The equations represent the drag force in heave (Eq. (11)) and drag moment in pitch (Eq. (12)) on one quarter of the structure so that the physical drag (left-hand side) is equal the drag in the FAST model (right-hand side). However, in order to achieve the right drag in both heave and pitch, an extra variable was introduced, i.e. the drag coefficient on the central virtual heave plate $C_{DHP_{FAST}}$:



$$\begin{aligned}
& \frac{1}{2} \rho C_{Da} A_{square} \dot{z} |\dot{z}| + \frac{1}{2} \rho C_D A_{pontoon} \dot{z} |\dot{z}| \\
&= \frac{1}{2} \frac{1}{2} \rho C_{Da_{FAST}} A_{col} \dot{z} |\dot{z}| + \int_0^L \frac{1}{2} \rho C_D D \dot{z} |\dot{z}| dr + \frac{1}{4} \frac{1}{2} \frac{1}{2} C_{DHP_{FAST}} A_{col} \dot{z} |\dot{z}|
\end{aligned} \tag{11}$$

$$\begin{aligned}
& \frac{1}{2} \rho C_{Da} A_{square} \dot{\theta} |\dot{\theta}| R^3 + \int_0^{\frac{L}{2}} \frac{1}{2} \rho C_D h_2 \dot{\theta} |\dot{\theta}| r^3 dr + \int_{R - \frac{h_2}{2}}^{R + \frac{h_2}{2}} \frac{1}{2} \rho C_D \frac{L}{2} \dot{\theta} |\dot{\theta}| r^3 dr \\
&= \frac{1}{2} \frac{1}{2} \rho C_{Da_{FAST}} A_{col} \dot{\theta} |\dot{\theta}| R^3 + \int_0^{\frac{L}{2}} \frac{1}{2} \rho C_D D \dot{\theta} |\dot{\theta}| r^3 dr + \int_{R - \frac{D}{2}}^{R + \frac{D}{2}} \frac{1}{2} \rho C_D \frac{L}{2} \dot{\theta} |\dot{\theta}| r^3 dr
\end{aligned} \tag{12}$$

Here R is the moment arm of 27.375 m from the centre of the floating substructure to the centreline of the pontoon and column. Furthermore \dot{z} is the heave velocity, $\dot{\theta}$ is the pitch velocity, A_{square} is the area of the square representing the bottom of each column and $A_{pontoon}$ is the area of the rectangular pontoons, $h_2 L$. A_{col} represents the cross-sectional area of the columns and D is the diameter of the cylindrical pontoons in the model, which is equal to the physical pontoon height h_1 . The last term on the right-hand side of Eq. (11) is the contribution from the virtual central heave plate, necessary to correctly model the drag in the heave direction. The integrals on both sides of Eq. (12) represent the contribution of the pontoons to the drag in pitch (the reader should note that one pontoon is parallel to the pitch axis, while the other is perpendicular, hence the integrals are different). For simplicity, only drag due to floating substructure motion is considered in Eqs. (11) and (12). A similar lumped approach for the wave forcing is more complicated due to the spatial variation of the wave velocity field, which is also frequency-dependent. The present approach was chosen as a first step to overcome the limitation to only cylindrical members in FAST. Equations (11) and (12) are solved simultaneously to yield values of 15.61 for $C_{Da_{FAST}}$ and 31.12 for $C_{DHP_{FAST}}$. A summary of the physical and model properties involved in the viscous drag on the bottom pontoon of the NAUTILUS-10 floating substructure is given in Table 17.

Table 17: Summary of drag properties for the pontoons of the NAUTILUS-10 floating substructure. The values on the right column have been determined to match the global drag in surge, heave and pitch for the physical structure

Property	Physical value	Model value	Colour in Figure 28
Pontoon height	1.5 m	1.5 m (diameter)	Red
Pontoon width	10.5 m	1.5 m (diameter)	Red
Transversal drag coefficient for pontoon	2.05	2.05	Red
Outer heave plate area	110.25 m ²	86.59 m ²	Blue
Outer heave plate drag coefficient	1.78	15.61	Blue
Central heave plate area	-	86.59 m ²	Green
Central heave plate drag coefficient	-	31.12	Green

